Science of the Total Environment 835 (2022) 155383

Contents lists available at ScienceDirect

Science of the Total Environment

journal homepage: www.elsevier.com/locate/scitotenv

SEM-EDS and water chemistry characteristics at the early stages of glacier recession reveal biogeochemical coupling between proglacial sediments and meltwater

Łukasz Stachnik [a,b,c,*], Jacob C. Yde [b], Kazimierz Krzemień [c], Łukasz Uzarowicz [d], Sławomir Sitek [e], Piotr Kenis [a,f]

[a] Department of Physical Geography, University of Wrocław, Wojciecha Cybulskiego Str. 34, 50-205 Wrocław, Poland
[b] Western Norway University of Applied Sciences, Department of Environmental Sciences, Røyrgata 6, 6856 Sogndal, Norway
[c] Jagiellonian University, Department of Geomorphology, Gronostajowa Str. 7, 30-387 Kraków, Poland
[d] Department of Soil Science, Institute of Agriculture, Warsaw University of Life Sciences – SGGW, Nowoursynowska Str. 159, Building 37, 02-776 Warsaw, Poland
[e] Institute of Earth Sciences, Faculty of Natural Sciences, University of Silesia in Katowice, Będzińska Str. 60, 41-200 Sosnowiec, Poland
[f] Łukasiewicz Research Network, PORT Polish Centre for Technology Development, Electron Microscopy Laboratory, Stabłowicka St.147, 54-066 Wroclaw, Poland

HIGHLIGHTS

- Strong coupling between water and sediment chemistry at early stage of recession
- Early deglaciation facilitates sulphide oxidation and carbonate dissolution.
- Glacier-derived physical weathering of iron sulphides enhances their oxidation.
- Sulphide oxidation enhanced formation of bioavailable iron oxides.

GRAPHICAL ABSTRACT

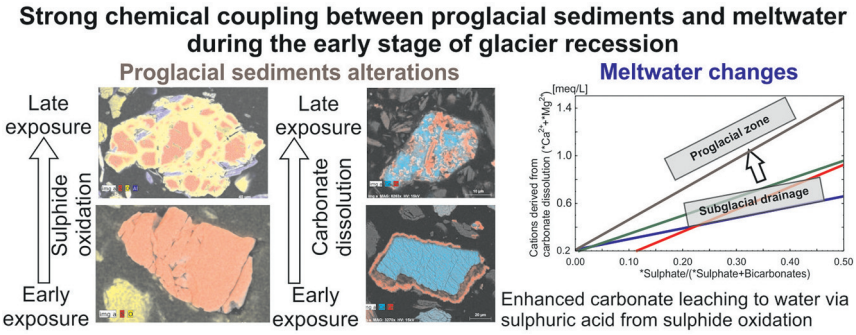

ARTICLE INFO

Editor: Daniel Alessi

Keywords:
Glacier recession
Silicate weathering
Sulphide oxidation
Iron cycle
Scanning electron microscopy
Chemical denudation
Land-based glacier

ABSTRACT

Most glaciers worldwide are undergoing climate-forced recession, but the impact of glacier changes on biogeochemical cycles is unclear. This study examines the influence of proglacial sediment weathering on meltwater chemistry at the early stages of glacier recession in the High Arctic of Svalbard. Scanning electron microscopy-energy dispersive X-ray spectroscopy (SEM-EDS) in combination with a wide range of geochemical analyses were used in this study. The SEM-EDS analyses of sediments collected in front of Werenskioldbreen show general degradation of pyrite and carbonate grains with age. The outer parts of pyrite grains have a gradual decrease in sulphur and gradual increase in iron oxides due to pyrite oxidation. This process was less advanced in the proglacial zone younger than 100 years compared to older sites such as the terminal moraine from the Little Ice Age. In both the proglacial zone and the terminal moraine, physical weathering of mineral grains, including formation of microcracks and microfractures, clearly enhanced pyrite oxidation. A consequence of proglacial sediment weathering is that the river chemistry is strongly affected by carbonate dissolution driven by sulphuric acid from sulphide oxidation. Also, reactive iron oxides, a product of sulphide oxidation, are mobilized in the proglacial zone. The results of this study show that proglacial weathering in the High Arctic of Svalbard is strongly coupled to river geochemistry, especially during the early stages of proglacial exposure after glacier recession.

* Corresponding author at: Department of Physical Geography, University of Wrocław, Wojciecha Cybulskiego Str. 34, 50-205 Wrocław, Poland
E-mail addresses: Lukasz.Stachnik@uwr.edu.pl (Ł Stachnik), Jacob.Yde@hvl.no (J.C. Yde), Kazimierz.Krzemien@uj.edu.pl (K. Krzemień), lukasz_uzarowicz@sggw.edu.pl (Ł Uzarowicz), Slawomir.S.Sitek@us.edu.pl (S. Sitek), piotr.kenis@port.lukasiewicz.gov.pl (P. Kenis).

http://dx.doi.org/10.1016/j.scitotenv.2022.155383
Received 11 January 2022; Received in revised form 12 April 2022; Accepted 14 April 2022
Available online 20 April 2022

1. Introduction

Glacierised basins influence global biogeochemical cycles as they are among the most dynamic environments in the hydrosphere and lithosphere (Arrigo et al., 2017; Bhatia et al., 2013; Hawkings et al., 2014, 2017; Hopwood et al., 2020; Hodson and Yde, 2022). Rapid glacier retreat and enhanced melt often lead to higher annual runoff resulting in the release of products originating from chemical and physical weathering such as suspended sediments and solutes including nutrients (Hasholt et al., 2018; Hawkings et al., 2014; Yde et al., 2014). However, rates of spatiotemporal changes in, and interactions between biogeochemical processes associated, with land-based glacier retreat, climate change and paraglacial biogeochemical ecosystem responses remain poorly understood (Anderson et al., 2017; Deuerling et al., 2019; Saros et al., 2019).

In the early stages of recession, glaciers affect biogeochemical cycles, particularly the carbon cycle, through a variety of pathways. For instance, consumption of atmospheric CO_2 increases via intensification of the carbon pump due to delivery of highly bioavailable micronutrients to aquatic environment (Gerringa et al., 2012; Hawkings et al., 2018; Hodson et al., 2017; Smetacek et al., 2012). Enhanced runoff and high glaciofluvial erosion in subglacial and proglacial environments increase downstream transport of vast amounts of micronutrients (Hawkings et al., 2014; Meire et al., 2016). Silicate dissolution and ion exchange appears to dominate in subglacial conditions beneath ice sheets (Andrews and Jacobson, 2018; Graly et al., 2014; Moore et al., 2013). Also, glacierised basins act as CO_2 and CH_4 sources to the atmosphere via processes such as dissolution of carbonates by sulphuric acid (Scribner et al., 2015; Torres et al., 2014, 2017; Torres et al., 2014; Zolkos et al., 2018) and respiration and organic carbon transformation in subglacial and proglacial environments (Bernasconi et al., 2011; Christiansen et al., 2021; Mavris et al., 2010).

During the early stages of glacier recession, the impact on the elemental fluxes associated with riverine transport is also affected. The formation of larger subglacial channels, as a consequence of increasing ablation rates may either reduce geochemical weathering as a result of shorter water residence time (Wadham et al., 2010b) or enhance solute-rich water release from isolated sites at the subglacial environment (Stachnik et al., 2016). Despite lower chemical weathering rates, solute mass fluxes from glacierised catchments tend to increase more than expected from runoff increase alone (Eiriksdottir et al., 2015) because adsorbed elements are also exported (Gíslason et al., 2006; Hawkings et al., 2014).

In the proglacial area, geochemical processes such as carbonate and sulphide dissolution and enhanced silicate weathering occur in the initial soils and fine-grained sediments due to the exposure of fresh mineral surfaces from glacial abrasion (Bernasconi et al., 2011; Kabala and Zapart, 2012; Zhou et al., 2016; Zolkos et al., 2018). At the early recession stage, vegetation succession, soil formation, and organic matter transformation favour a stronger binding of weathering products to organic compounds (Cooper et al., 2002; Deuerling et al., 2018; Szymański, 2017, 2019, 2022; Wietrzyk-Pełka et al., 2020). This process may moderate some of the additional solute flux associated with deposition of suspended sediments on proglacial outwash plains and proglacial river terrace development associated with glacier retreat.

Despite their great potential, scanning electron microscopy (SEM) techniques have rarely been applied to identify mineralogical transformations in the proglacial zone. Available studies show that chemical weathering of sulphide minerals leads to the formation of iron sulphate crusts (Rzepa et al., 2019) and Fe oxide rims in the late stages of weathering (Auqué et al., 2019; Kwaśniak-Kominek et al., 2016). Also, a connection between sulphide oxidation in sediments and pore water quality in moraines has been observed (Auqué et al., 2019; Kwaśniak-Kominek et al., 2016). For silicates, mineralogical analyses have shown signs of pronounced physical weathering such as the defragmentation of biotite and plagioclase crystals (Mavris et al., 2010). However, there is little knowledge on the rates of chemical weathering of minerals along chronosequences in glacier forelands. Apart from glacierised basins, sulphide oxidation chronosequences have been investigated using mineralogical techniques in laboratory analyses (Weber et al., 2004), and in natural and technogenic soils (Uzarowicz and Skiba, 2011; Uzarowicz, 2013).

This study examines the hypothesis that proglacial chemical weathering is associated with meltwater chemistry in the proglacial zone during the early stage of glacier recession. We used SEM-EDS techniques in combination with a wide range of geochemical analyses to characterize the extent of chemical and physical weathering. The relationship between geochemical properties of proglacial sediment and water chemistry is pivotal in forecasting of changes in biogeochemical processes associated with land-based glacier shrinkage. The results provide a basis for discussing the long-term effects of glacier recession on biogeochemical cycles.

2. Study area

The study area is located in the foreland of Werenskioldbreen in the southwestern part of Svalbard (77.08 °N, 15.25 °E) (Fig. 1). The entire basin covers an area of 44.1 km^2 with a glacierised area of 27.4 km^2 (Hagen et al., 1993). The mean annual glacier surface mass balance was −100 mm in water equivalent for 1959–2002 (Grabiec et al., 2012; Table 1). Werenskioldbreen occupies a wide, flat-bottomed valley with a north-western aspect, surrounded by mountain ridges with altitudes of ~600–700 m a.s.l. and a mean slope of ~6° (Table 1).

At the Polish Polar Station in Svalbard, about 12 km southeast of Werenskioldbreen, the mean monthly air temperature was <5 °C during the ablation season (July–September) and the mean annual precipitation was ~430 mm during the period 1979–2009 (Marsz and Styszyńska, 2013). The mean monthly air temperature in the Werenskioldbreen basin tends to be slightly higher by an average of ~0.6 °C (up to ~1.0 °C for April and August) than at the Polish Polar Station (Pereyma et al., 2013) (Table 1).

The bedrock consists of the Hecla Hoek succession in a contact zone of three Proterozoic blocks (Eimfjellet group, Deillega group, Jens Erikfjellet formation). The Eimfjellet group comprises amphibolite, quartzite, and chlorite schists. Phyllites with quartzite and calcareous and chlorite schists are observed in the Deillega group, while the Jens Erikfjellet formation consists of muscovite-carbonate-quartz and carbonate-chlorite-quartz schists (Czerny et al., 1992, 1993). Sediments and bedrock of the Werenskioldbreen basin consist of minerals such as quartz micas (muscovite and paragonite), chlorite, feldspars (plagioclases and K-feldspar), and epidote (Czerny et al., 1992, 1993; Stachnik et al., 2019).

3. Methods

3.1. Field methods

3.1.1. Sediment and soil sampling

Soil and sediment samples (N = 23) were collected along the chronosequence in front of Werenskioldbreen in three different areas (Fig. 1): The early exposed proglacial zone (profiles 023, 020, 022, 016, 014, 006; hereafter “proglacial zone I"), the advanced exposed proglacial zone (profiles 021, 011, 008, 002, 001; hereafter “proglacial zone II"), and at the terminal moraine (profiles 017, 012). The sampling sites in proglacial zone I were deglaciated after 1973 (27–44 years exposure age), while proglacial zone II was deglaciated before 1957 (>60 years exposure) (Ciężkowski et al., 2018) and the terminal moraine was likely formed at the end of the Little Ice Age (LIA) during the late-19th or early-20th century (>100 years ago).

At each sampling site, a profile was excavated to a depth between 0.2 and 1.0 m depending on what was possible due to boulder content. Two or three sediment samples were usually collected from different layers in the vertical profiles (Fig. 2). For sampling at the vicinity of the glacier (e.g., profiles 022, 023, 024), only surface samples (0–0.1 m) were collected.

3.1.2. Water sampling

The fieldwork was conducted during the entire ablation season in 2011, which was divided into three parts based on hydrograph characteristics:

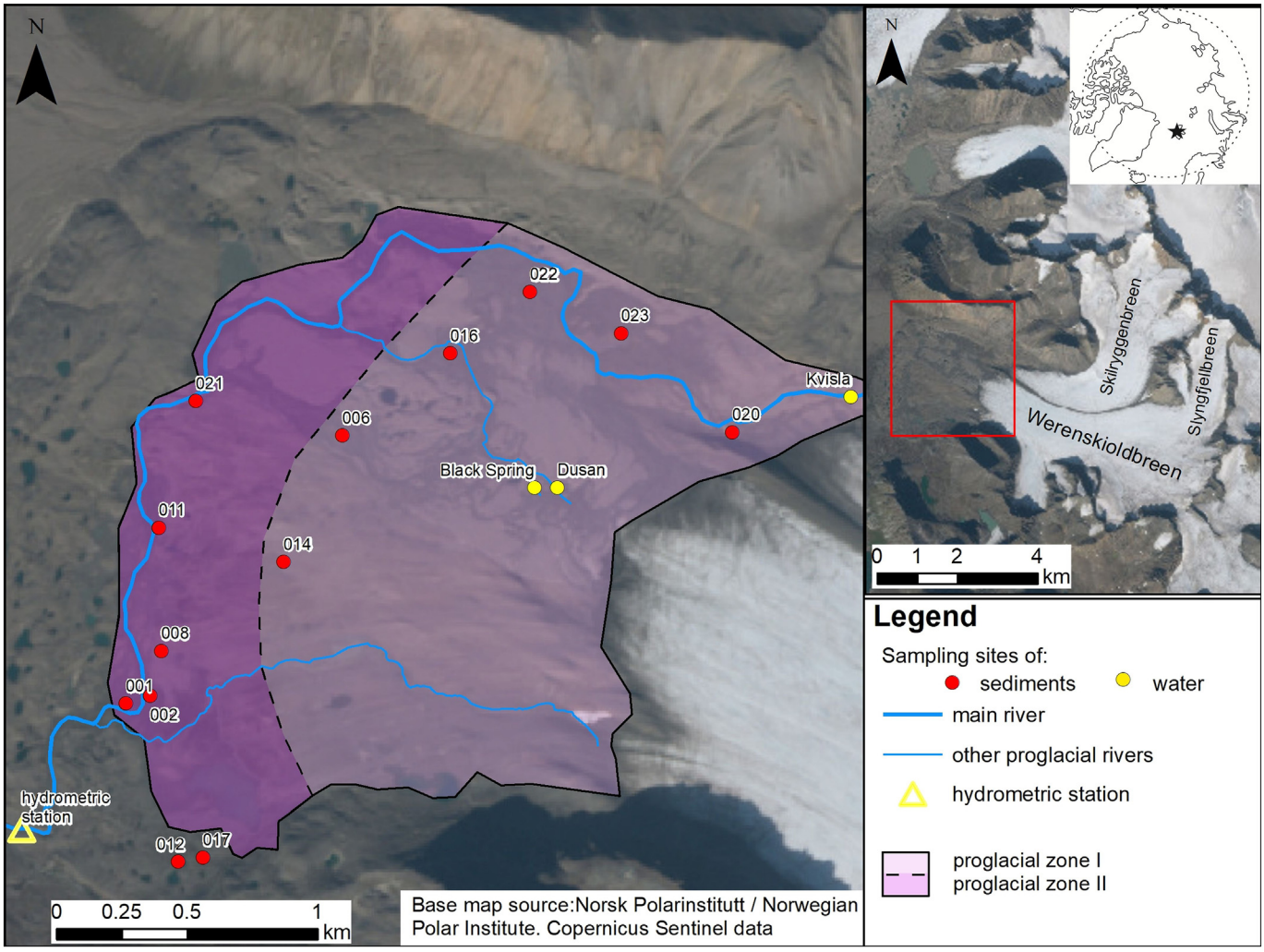

Fig. 1. Study area (image taken on 24.08.2013, scene ID: LC82110052013236LGN01, Landsat 8 true colour). The yellow dots, red dots, and yellow triangles represent water sampling sites, sediment sampling sites, and hydrometric station, respectively. Kvisla is a channelized outflow, and the Dusan and Black spring are subglacial artesian outflows. The early stage of recession (proglacial zone I), the advanced stage of recession (proglacial zone II), and the final stage (terminal moraine) are shown.

The early ablation season (May 12–June 18, 2011), the peak flow period (June 19–September 10, 2011) and the late ablation season (September 11–25, 2011) (Stachnik et al., 2016). Meltwater samples were collected at a channelized glacier portal (Kvisla $N = 28$), at subartesian outflows (Dusan $N = 24$, Black spring $N = 22$) and at the downstream hydrometric station (HSW) ($N = 183$). Details regarding sample treatment and storage are described by Stachnik et al. (2016).

Table 1
Local conditions in the Werenskioldbreen. [1] VI, VII, VIII, IX denote mean air temperature for June, July, August, September, respectively. [2] w.e. denotes water equivalent.

Characteristics	Werenskioldbreen
Catchment area	44 km^2 (61.3% glacier cover)
Geographical position	77.08°N, 15.25°E
Elevation drop (min-max altitude)	944 m (5-949 m a.s.l.)
Mean slope of basin	5.9°
Bedrock	Phyllites, quartzites, metamorphic schists, amphibolites
Ore minerals	Pyrite, chalcopyrite, galena
Silicates	Albite, chlorite, micas, hornblenda, amphibole, biotite,
Carbonates	Siderite, ankerite, dolomite, calcite
T_{air} VI, VII, VIII, IX[1]	1.9; 4.4; 4.1; 1.4 °C
Mean annual precipitation	434.4 mm (1979-2009)
Mean annual mass balance	−100 mm in w.e.[2] (1959–2002)

3.1.3. Discharge measurements

The area-velocity method was used to determine discharge in glacial outflows draining Werenskioldbreen (Majchrowska et al., 2015; Stachnik et al., 2016). In short, discharge was calculated based upon rating curves and water level measurements during the fieldwork period. Discharge was determined using the cross-sectional area and water velocity with different techniques depending on the prevailing conditions. The current-meter method was mainly used during the peak flow period and late ablation season. Only in May 2011, the float method was applied owing to difficulties with other types of discharge measurements in snow-bank channels.

3.2. Sediment analyses

3.2.1. XRD analyses

Mineral composition of the sediment samples was determined using powder X-ray diffraction method (XRD). The fine material (<2 mm) from the samples were ground and powders were analysed with the use of a Bruker AXS D5005 diffractometer equipped with a KRISTALLOFLEX®

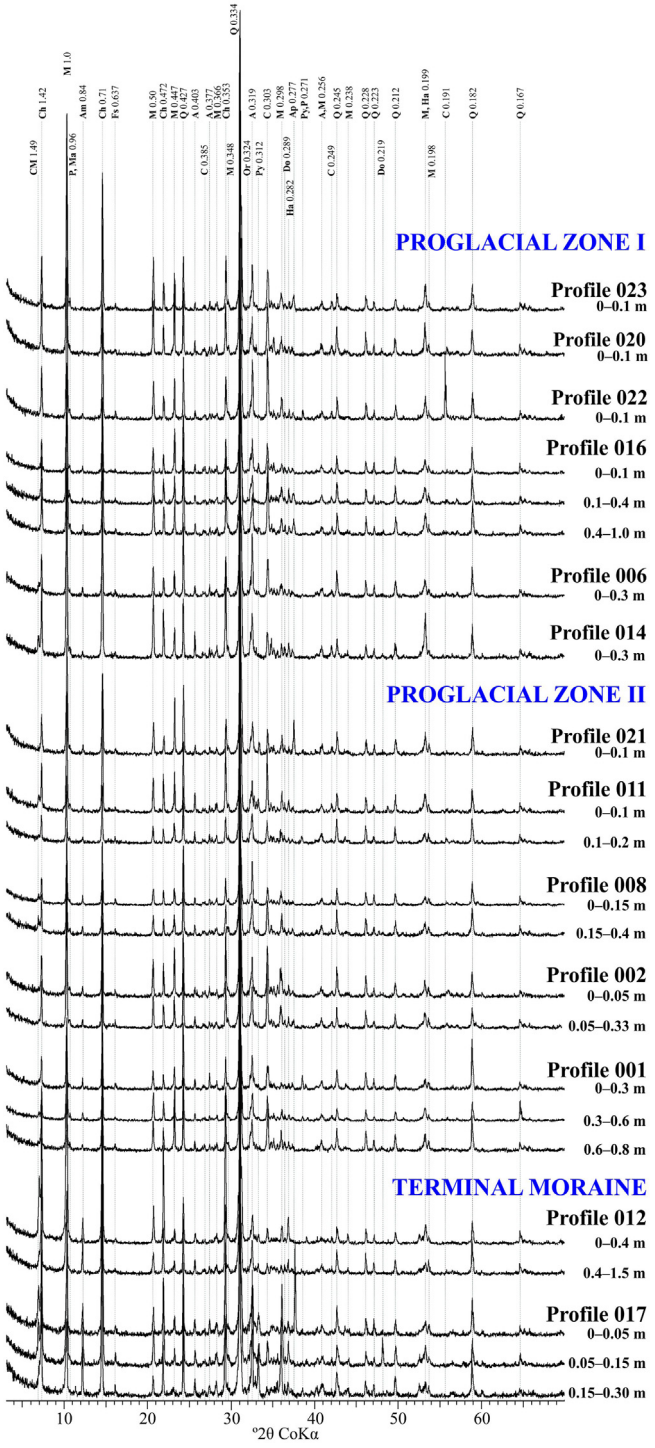

Fig. 2. Mineral composition of selected sediments from the proglacial zone and terminal moraine in the Werenskioldbreen catchment based on XRD analyses. Mineral symbols: A – albite, Am – amphibole, Ap – apatite, C – calcite, Ch – chlorite, Do – dolomite, Fs – feldspars (generally), M – muscovite, Ma – marcasite, Or – orthoclase, P – paragonite, Py – pyrite, Ma – marcasite, Q – quartz, Ha – halite. The d values (in italics) are in nm.

760 X-ray generator, a vertical goniometer, a 1 mm divergence slit, a 2 mm anti scatter slit, a 0.6 detector slit, and a graphite diffracted-beam monochromator. CoKα radiation was used with the applied voltage of 40 kV and 35 mA current. Random mounts of the ground materials were scanned from 3 to 70°2θ at a counting time of 2 s per 0.01° step on a rotating stage. XRD analyses were performed at the Department of Soil Science, Institute of Agriculture, Warsaw University of Life Sciences – SGGW, Poland. The mineral composition of each sample determined by XRD is listed in the supplementary materials (Table A.1).

3.2.2. SEM-EDS and QEMSCAN® analyses

Scanning electron microscopy – energy dispersive X-ray spectroscopy (SEM-EDS) studies were conducted to investigate the microchemical effects of mineral weathering. Samples of glacial sediments and soils were examined (1) as blocks embedded in resin, which enabled SEM-EDS analysis of cross-sections of minerals and (2) as powder poured onto carbon tape, which enabled analysis of the morphology of mineral grains. The samples were carbon coated prior to the analyses. Samples were imaged using a Quanta 650 FEG scanning electron microscope (SEM) Thermo Fisher Scientific (formerly the FEI Company) equipped with two EDS detectors (Bruker Inc.). The EDS detectors permitted examination of the elemental composition of the samples at the microscopic scale. Imaging was performed in high vacuum mode using an accelerating voltage of 20 kV. Images were recorded in back-scattered electron (BSE) mode, which yielded information on the variability of the chemical composition, and in secondary electron (SE) mode, which provided details of the mineral surface topography.

Special QEMSCAN® software was used to quantitatively estimate the mineral composition in the samples. Tens of thousands of grains were measured in each sample at 2 μm spacing with accelerating voltage of 25 kV. The scanned particles were classified into the appropriate mineral groups. The methodology of sample preparation and measurements has been described in detail by Kenis et al. (2020).

3.3. Water analyses and hydrochemical calculations

Raw water chemistry data were obtained from earlier work (Stachnik et al., 2016) and used in a new approach by focusing on the influence of sediment geochemistry on meltwater chemistry at the early stage of glacier retreat. The analytical procedures for determination of major ions were described by Stachnik et al. (2016). Briefly, the concentrations of major ions were determined by the ion chromatography method (Methrom Compact IC 761). The analytical detection limits were as follows: Ca^{2+} (0.5 μeq/l), Mg^{2+} (0.8 μeq/l), Na^{+} (0.4 μeq/l), K^{+} (0.3 μeq/l), SO_4^{2-} (0.2 μeq/l), Cl^{-} (0.3 μeq/l) and NO_3^{-} (0.2 μeq/l) (Stachnik et al., 2016). The respective precisions for the ion concentration analyses were less than 1%, while the precisions of certified reference materials (Analytical Reference Material Rain-97 and Reference Material No. 49 (BCR-409) were < 10%, except for Na^{+} (12%), K^{+} (18%), and Cl^{-} (22%) (Stachnik et al., 2016). The charge balance errors were on average less than 3% (Stachnik et al., 2016).

The alkalinity was determined using a Methrom 702 SM Titrino instrument. Given the pH value of the meltwater, it is assumed that alkalinity is equal to the concentration of bicarbonate. The ion concentrations (SO_4^{2-}, Ca^{2+}, Mg^{2+}, Na^{+}, K^{+}) were corrected for atmospheric inputs using the ion to Cl ratio in seawater (eq. 1; (Holland, 1978) as described in previous literature on hydrochemistry in glacierised basins (Hodson et al., 2000; Stachnik et al., 2016). The corrected ions are marked with an asterisk (*).

$$^{*}X = {}^{total}X - {}^{total}Cl^{-}\ (X:Cl^{-})_{seawater} \quad (1)$$

where*X – concentration of ion X corrected for sea-salts,^{total}X – total concentration of ion X in a sample,^{total}Cl – total concentration of Cl^{-} ion in a sample,$(X{:}Cl^{-})_{seawater}$ – ratio of ion X:Cl^{-} in seawater (Holland, 1978)

The sulphate mass fraction (SMF) is an indicator of chemical weathering used to distinguish sulphide oxidation, carbonation (dissolution of carbonate or silicate minerals by carbonic acid), and efflorescent salt dissolution (Eq. 2). The SMF equal to 0.5 corresponds to predominating sulphide oxidation coupled to carbonate dissolution; SMF lower or higher than 0.5 indicates carbonation of carbonates and silicates or a variety of processes (sulphide oxidation coupled to silicate weathering, carbonate precipitation

and Ca, Mg efflorescent salt dissolution), respectively (Cooper et al., 2002; Tranter et al., 2002).

$$SMF = {}^{*}SO_4^{2-} / \left({}^{*}SO_4^{2-} + HCO_3^{-}\right) \quad (2)$$

where SMF – sulphate mass fraction, $^{*}SO_4^{2}$ – the concentration in μeq L^{-1} of sulphate, corrected for atmospheric input, HCO_3^{-} – the concentration in μeq L^{-1} of bicarbonate.

3.4. Runoff and mass flux calculations

The mean total dissolved solids (TDS) corrected for atmospheric input (Eq. 1) weighted by discharge was used to calculate solute mass fluxes. The TDS is the sum of $^{*}Ca^{2+}$, $^{*}Mg^{2+}$, $^{*}Na^{+}$, $^{*}K^{+}$, HCO_3^{-}, $^{*}SO_4^{2-}$, and $^{*}Cl^{-}$. Discharge-weighted mean TDS was multiplied by runoff from the ablation season to estimate the total solute mass flux corrected for atmospheric input. Runoff is the sum of daily runoff measured at the hydrometric station. Details about the runoff and mass flux calculation for May–September 2011 at Werenskioldbreen are described by (Stachnik et al., 2016).

3.5. Statistical analyses

Relationships between hydrochemical variables were analysed by fitting the linear regression and calculation correlation coefficients. To check assumptions of linear regression and Pearson's correlation coefficient, we performed residual analyses including normality (Kołmogorow-Smirnov and Shapiro-Wilk tests) and lack of autocorrelation (Durbin-Watson test) of residuals, and checked the linearity of relationships. If residual distribution was non-normal, log transformation was performed to parameters. Also, we checked the relationships between hydrochemical parameters using a non-parametric test (Spearman rank's correlation) for those linear regression models, which did not have normal distribution.

4. Results

4.1. XRD analysis

The major mineral phases of sediments in the proglacial area of Werenskioldbreen were silicates/aluminosilicates (e.g., quartz, mica, chlorite, feldspar – plagioclase and orthoclase) followed by a minor content of carbonate (dolomite and calcite) (Fig. 2, Table A.1). In some samples, Fe sulphides (e.g., marcasite, pyrite), halite and apatite were detected. Selected grains with partly weathered mineral surfaces are shown in Fig. A.1 as examples for grain morphology. Carbonates are more abundant in samples from the proglacial zone than in samples from the terminal moraine. This is shown by lower intensity of carbonate peaks in XRD patterns in samples from the terminal moraine in comparison to samples from the proglacial zone (Fig. 2) suggesting lower quantities of carbonates in the former site. In general, the mineral composition of the proglacial samples is consistent with the mineral composition of subglacial sediments from Werenskioldbreen (Stachnik et al., 2019).

4.2. SEM-EDS analysis

SEM-EDS analysis provided insights into the morphology of minerals in the sediments occurring in the proglacial areas of Werenskioldbreen (Fig. 3), as well as into the progression of chemical weathering and the direction of mineral transformations (Figs. 4, 5, 6). In the High Arctic proglacial environment of Werenskioldbreen, less weathering-resistant minerals (calcite [Fig. 3C], dolomite [Fig. 3D], and biotite [Fig. 3E]) and more weathering-resistant minerals (albite [Fig. 3F], quartz [Fig. 3G], and ilmenite [Fig. 3H]) were all exposed to intense physical weathering. Microcracks were common in calcite, quartz, and dolomite mineral grains, whereas muscovite and biotite mineral grains showed exfoliation patterns (Fig. 3).

The SEM-EDS analyses revealed that Fe sulphides were subjected to intense weathering resulting in the formation of Fe oxides on the surfaces of sulphide grains (Figs. 4, A.2). Grains of massive sulphides (Fig. 4E, F, G, H,

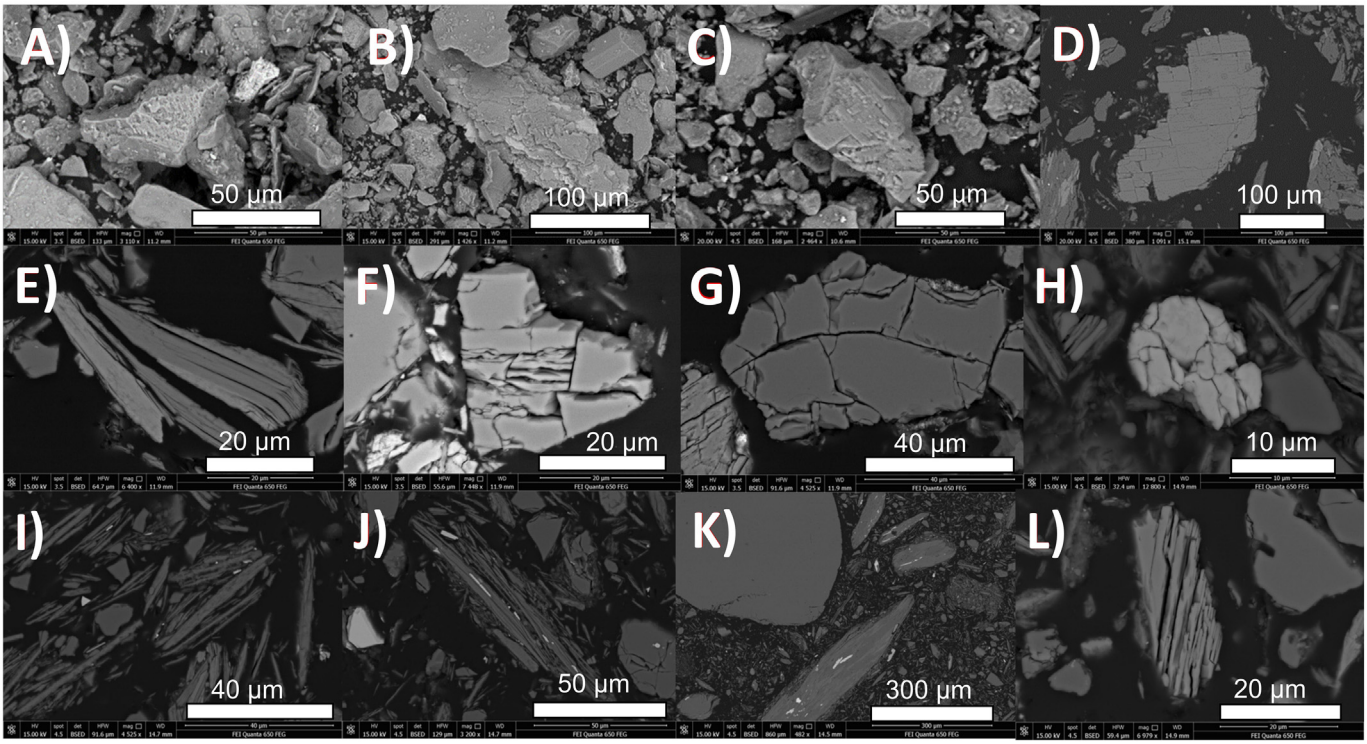

Fig. 3. Selected mineral phases occurring in sediments in the vicinity of Werenskioldbreen: A – albite, B – muscovite, C – calcite, D – dolomite, E – biotite, F – albite, G – quartz, H – ilmenite. All images are shown in back-scattered electron (BSE) mode.

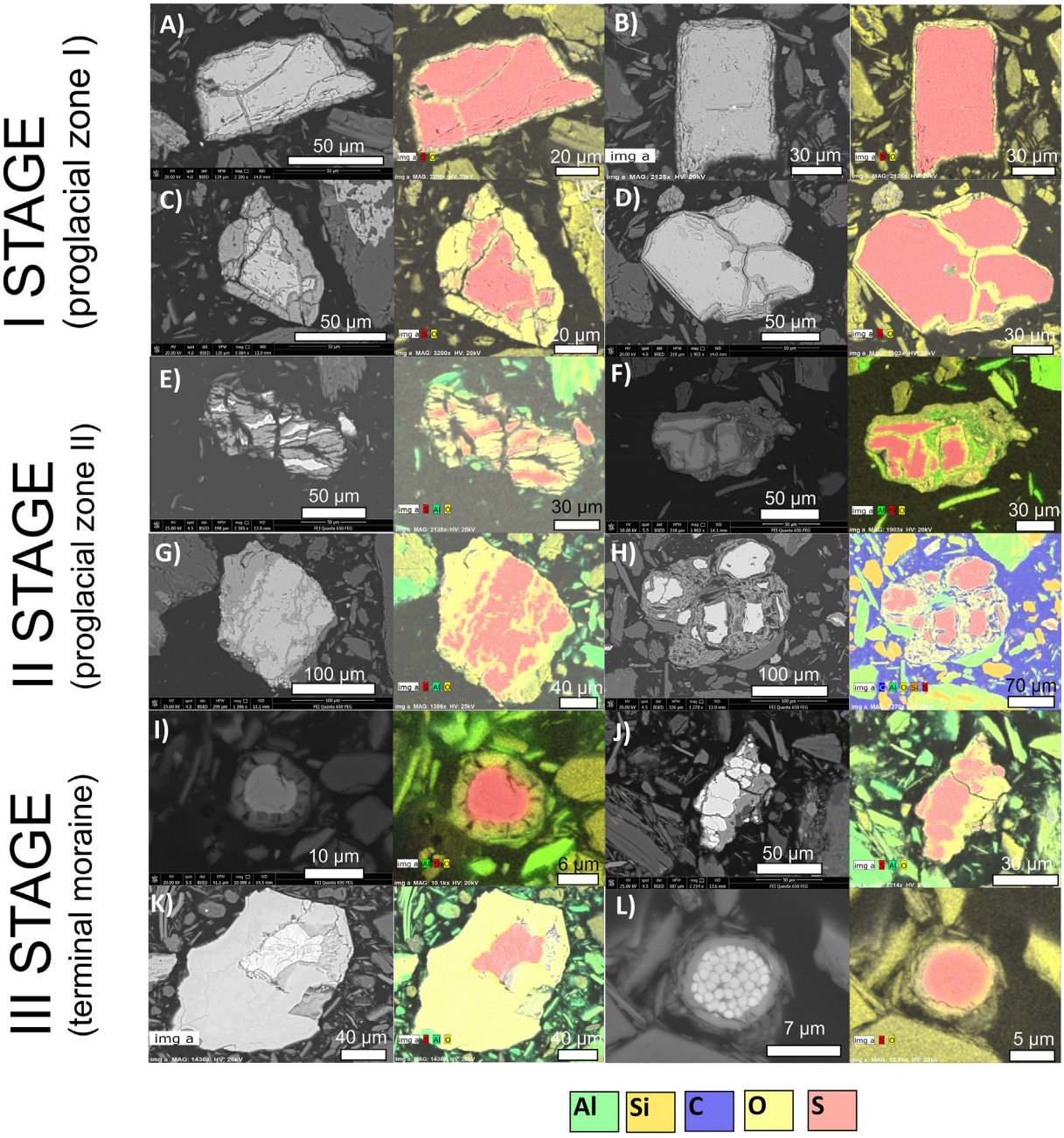

Fig. 4. Fate model of iron sulphides and iron oxides in the chronosequence of Werenskioldbreen: A-D) proglacial zone I (profile 023), *E*-H) proglacial zone II (profile 011), I-L) terminal moraine (profile 012).

A.3, A.4) were dominant and occurred together with the framboidal form of Fe sulphides (Fig. 4I, L, A.2). Along the proglacial chronosequence, weathering of Fe sulphides changed from being poorly weathered in proglacial zone I (Figs. 4A-D), through advanced oxidation in the proglacial zone II (Fig. 4 *E*-H) to being intensely weathered in the terminal moraine (Fig. 4 I-L). The sulphur content clearly decreased along the chronosequence with increase of oxygen in the oxidation rim as seen by comparing Fig. 4B with Fig. 4K. Also, physical features such as microcracks facilitated grain oxidation (Fig. 4D, H). The products of Fe sulphide weathering consisted of (1) pseudomorphs of Fe oxides after Fe sulphides (Fig. A.5), (2) aggregates cemented by Fe oxides (Fig. A.6), (3) secondary Fe oxide coatings around mineral grains (e.g., carbonates) (Fig. A.7), and (4) Fe oxides, likely goethite (Fig. A.8). The aggregates and coatings were frequently observed in proglacial zone II.

4.3. Chemical composition of sulphides and their weathering products

The chemical composition of Fe sulphides in the proglacial sediments from Werenskioldbreen is very similar along the chronosequence (Fig. 5). The relative contents of Fe, S and O in Fe sulphides based on semiquantitative EDS analyses were 54.1–60.0 wt% Fe (av. 58.7 wt%, $n = 10$); 25.7–39.4 wt% S (av. 35.5 wt%, n = 10); 1.1–17.2 wt% O (av. 5.1 wt%, n = 10) (Table 2). The highest concentrations of O were detected in framboidal Fe sulphides (Fig. 5E). EDS analysis of Fe sulphides also revealed trace concentrations of Si, Al, and Ca (up to 1.2, 0.8 and 0.7 wt% respectively).

Fe oxides, products of Fe sulphide weathering, were characterized by diverse chemical compositions. They contained, on average, 58.80 wt% Fe (range 44.3–63.8 wt%, $n = 15$), 33.4 wt% O (range 22.8–39.1%, n =

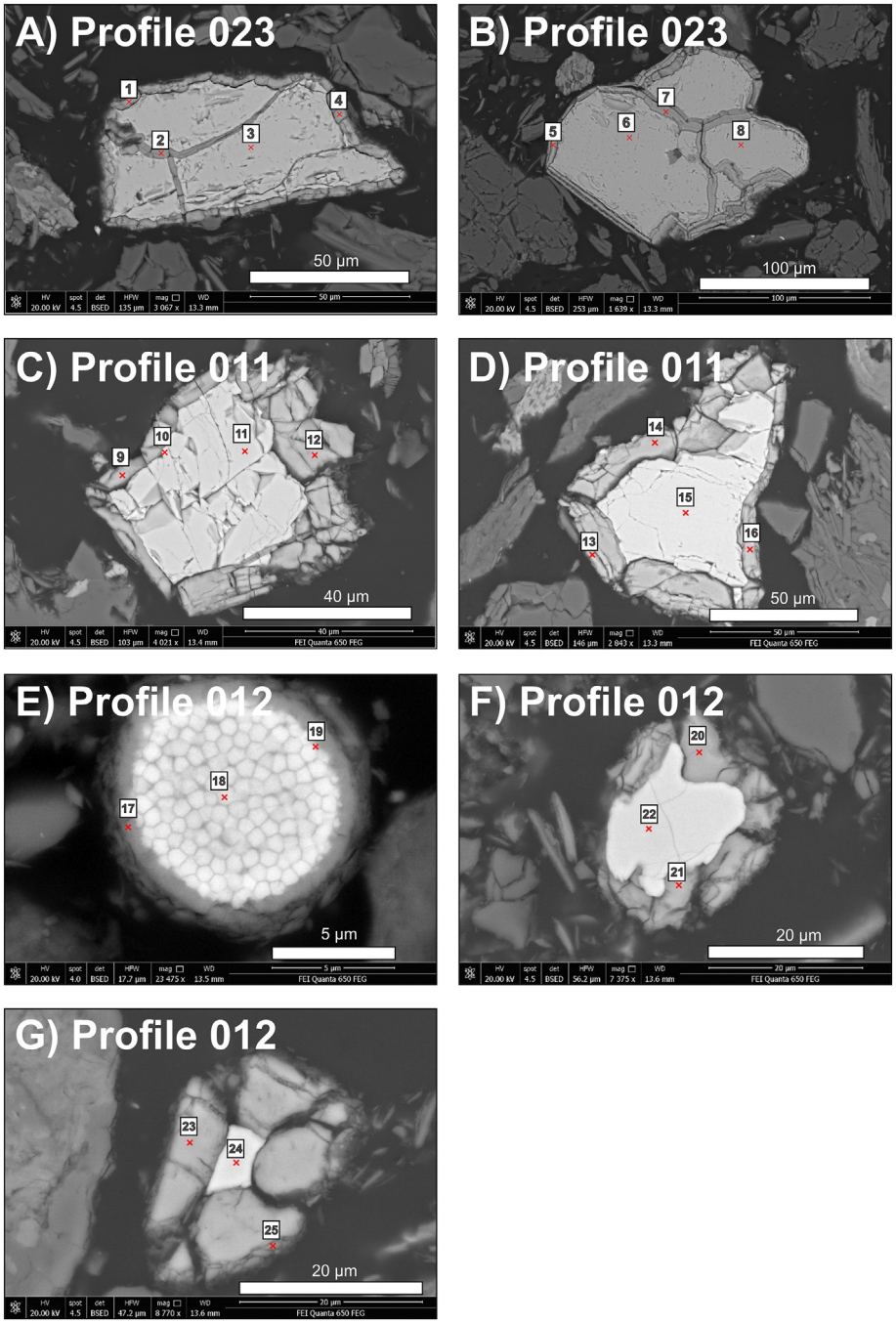

Fig. 5. BSE images of selected mineral grains with the points of EDS analyses shown in Table 2. A – poorly weathered massive Fe sulphide surrounded by a thin, sulphur-rich Fe oxide rim (Profile 023), B – poorly weathered massive Fe sulphide surrounded by a laminated Fe oxide rim (Profile 023), C – partly weathered massive Fe sulphide surrounded by a Fe oxide rim (Profile 011), D – partly weathered massive Fe sulphide surrounded by an Fe oxide rim (Profile 011), E – framboidal Fe sulphide surrounded by an Fe oxide rim; the Fe sulphide crystals are poorly weathered (Profile 012), F – partly weathered massive Fe sulphide surrounded by an Fe oxide rim (Profile 012), G – strongly weathered massive Fe sulphide surrounded by an Fe oxide rim (Profile 012).

15), and 1.9 wt% S (range 0.3–11.9 wt%, n = 15). The highest concentrations of S were detected in Fe oxide rims of poorly weathered Fe sulphides (Fig. 5A), as well as in Fe oxides occurring within weathered framboids (Fig. 5E). Fe oxides in sediments from Werenskioldbreen also contained, on average, 2.5 wt% Si (range 0.6–11.7%, n = 15), 0.8 wt% Al (range 0.01–5.1%, *n* = 14), 1.9 wt% Ca (range 0.4–3.4 wt%, n = 15), 0.30 wt% Mg (range 0.04–1.1 wt%, *n* = 12), and 0.6 wt% K (range 0.02–1.8%, *n* = 5) (Table 2). The highest concentrations of Si, Al, Mg and K were detected in Fe oxides within weathered framboids (Fig. 5E). The EDS analyses also showed that Fe oxides contain low concentrations of Na, Cl, P, Ti and Co (Table 2).

Line SEM-EDS profiles showed a clear pattern in changes of elemental content in the Fe sulphide grains in the proglacial area of Werenskioldbreen. Massive Fe sulphides from proglacial zone I (profile 012) had high S content in the entire grain, but the S content decreased towards the rim and in microcracks and microfractures (Figs. 6A-B, A.9). Along with peripheral S decrease, Fe and O concentrations increased showing higher content of Fe oxides. This pattern is also common for proglacial zone II and the terminal moraine (profiles 011 and 012, respectively), but the S content changes more abruptly and is replaced by Fe and O (Figs. 6C-E). Despite high S content in the terminal moraine, grain size is much smaller as compared with both proglacial zones (Figs. 4I, 6E, F). In

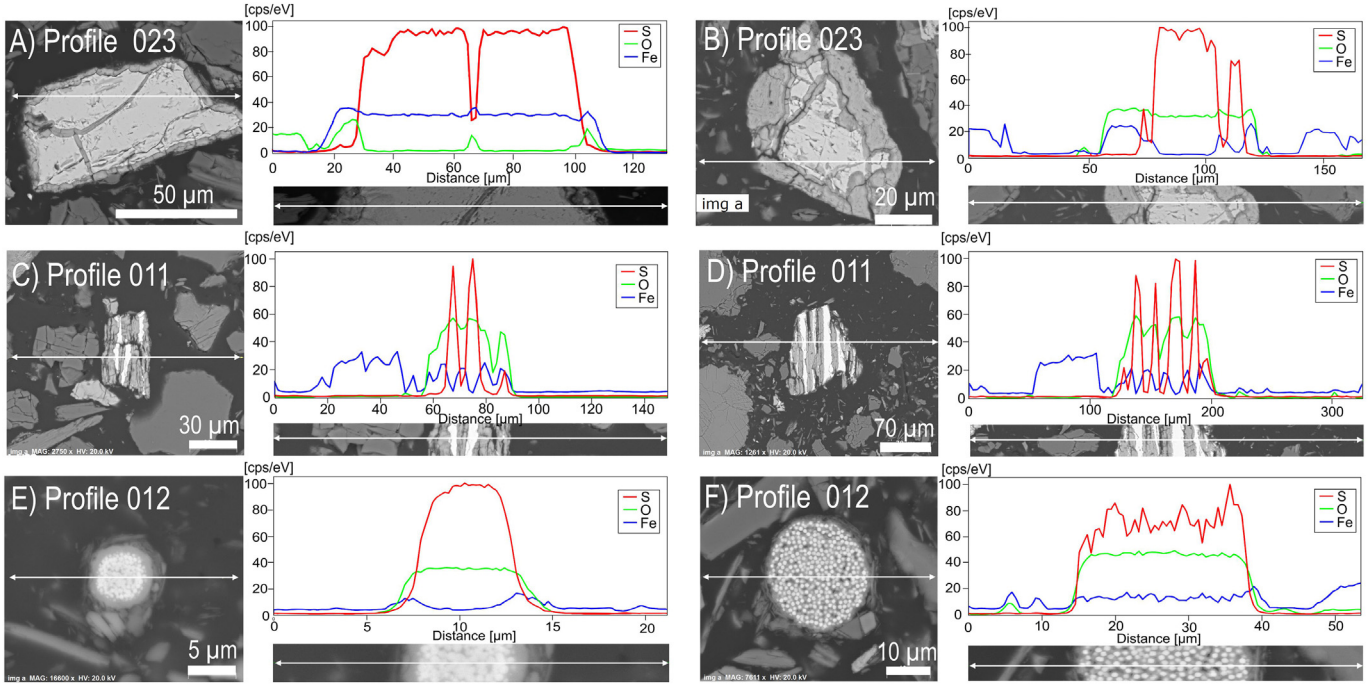

Fig. 6. BSE images of selected iron sulphide grains in chronosequence of the proglacial zone of Werenskioldbreen with the lines (elements Fe, S, O) of EDS analyses. A-B) proglacial zone I CD) proglacial zone II, E-F) terminal moraine.

addition, the weathering pattern is clearly visible in the decrease of sulphide content starting from the proglacial zone I through the proglacial zone II to the terminal moraine as shown by the results of the QEMSCAN® analyses (Fig. 7).

4.4. Water chemistry, runoff, and mass fluxes

The ion chemistry of subglacial and proglacial water was dominated by bicarbonate and calcium ions supplemented by sulphates and magnesium ions (Table A.2; (Stachnik et al., 2016). For the hydrometric station, most of the ions had higher concentration (734 ueq/L, 148 ueq/L, 190 ueq/L, 214 ueq/L, 666 ueq/L for Ca^{2+}, Mg^{2+}, Na^{+}, Cl^{-}, HCO_3^{-}, SO_4^{2-}, respectively; Table A.2) than samples from subglacial outflows. Water pH was higher by ~0.5 at the subglacial outflow (pH = 8.93) than at the hydrometric station. The SMF index showed generally higher values than 0.35 during the early and late parts of ablation season, whereas the $(*Na^{+} + *K^{+}):(*Ca^{2+} + *Mg^{2+})$ ratio was on average lower than 0.02 (Table 3).

Linear regression models ($*Na^{+} + *K^{+}$ vs. HCO_3^{-}, $*Na^{+} + *K^{+}$ vs. $*SO_4^{2-}$, $*Ca^{2+} + *Mg^{2+}$ and SMF) had normal distribution of residuals according to Kołmogorow-Smirnov test. After log transformation, the residuals of regression in one regression model ($*Na^{+} + *K^{+}$ vs. HCO_3^{-} from the peak flow season) showed a normal distribution (Table A.3). Residuals from regression models for low numbers of samples ($N < 30$) including the relationship between $*Ca^{2+} + *Mg^{2+}$ and SMF for Black Spring and Kvisla, and relationships from the hydrometric station at the late part of ablation season ($*Na^{+} + *K^{+}$ vs. HCO_3^{-}, $*Na^{+} + *K^{+}$ vs. $*SO_4^{2-}$, $*Ca^{2+} + *Mg^{2+}$) showed a normal distribution according to the Shapiro-Wilk test. Most of the residuals from regression models indicated a lack of autocorrelation excluding two regression models ($*Na^{+} + *K^{+}$ vs. HCO_3^{-}, $*Na^{+} + *K^{+}$ vs. $*SO_4^{2-}$ at the hydrometric station during the peak flow). All linear regression models were statistically significant ($p < 0.05$). In addition, parametric (Pearson's, hereafter r) and non-parametric (Spearman's rank order, hereafter rho) correlation coefficients showed similar range of values (Table A.3).

The slopes of the ion associations $*Na^{+} + *K^{+}$ vs. $*SO_4^{2-}$ and $*Na^{+} + *K^{+}$ vs. HCO_3^{-} and their seasonal changes were similar at the hydrometric station. Both slopes increased from the early part of the ablation season (~0.025) to the late part of the ablation season (>0.100), and the highest Pearson's correlation coefficients ($r > 0.7$, rho >0.7) were noted for the latter part (Table 4, Figs. 8A-B). Also, the Pearson's and Spearman's rank order correlation coefficients between $*Ca^{2+} + *Mg^{2+}$ and SMF were positive and strong for the hydrometric station ($r = 0.83$, rho = 0.82) compared

Table 2
Chemical composition (wt. % of each element) of mineral phases shown in Fig. 5 based on semiquantitative EDS analyses. Numbers from 1 to 25 indicate points in Fig. 5.

Element	1	2	3	4	5	6	7	8	9	10	11	12	13	14	15	16	17	18	19	20	21	22	23	24	25
Fe	59.2	63.0	58.7	62.9	61.4	59.2	63.4	58.8	63.8	59.5	59.8	62.2	61.5	63.3	60.0	58.8	44.3	59.5	54.1	57.4	58.0	58.3	56.7	59.1	46.3
O	33.5	31.4	1.7	32.2	34.9	1.7	34.6	1.9	30.6	10.9	1.1	34.1	34.7	32.5	1.3	37.4	22.8	9.1	17.2	34.7	34.0	3.8	34.3	2.0	39.1
S	2.2	3.0	39.4	1.6	1.1	38.9	0.3	39.1	0.9	28.3	38.9	0.3	0.4	0.4	38.5	0.7	11.9	30.3	25.7	2.0	2.1	37.5	0.5	38.5	0.5
Si	1.8	0.8	0.1	1.2	1.3	0.1	0.6	0.1	1.7	0.4	0.1	1.2	1.7	1.2	0.1	1.3	11.7	0.3	1.2	2.4	2.3	0.2	3.0	0.2	5.8
Al	0.8	0.1	–	0.2	0.1	0.1	0.0	0.2	0.7	0.2	0.1	0.2	0.2	0.1	0.1		5.1		0.8	0.2	0.1		0.7	0.2	2.9
Ca	2.1	1.7	–	1.7	0.7		0.4		2.3	0.7	0.0	2.1	1.4	2.5		1.9	0.4	0.2	0.2	3.2	3.4	0.3	3.4		2.1
Mg	0.2	0.0	–	0.2	0.3		0.5		–	–	–	–	0.1	0.1			1.1		0.5	0.2	0.2		0.2		0.6
K	–	–	–	–	-	–	–	–	–	–	–	–	0.1	0.0			1.8		0.1				0.1		1.0
Na	–	–	–		0.2	–	–		–	–	–	–													
Ti	–	–	–	–	-	–	–	–	–	–	–	–					0.3		0.2						0.5
Co	–	–	–	–	-	–	–	–	–	–	–	–						0.6					0.9		
P	–	–	–	–	-	–	–	–	–	–	–	–											0.2		0.1
Cl	–	–	–	–	-	–	–	–	0.1				0.1	0.0			0.7								1.2

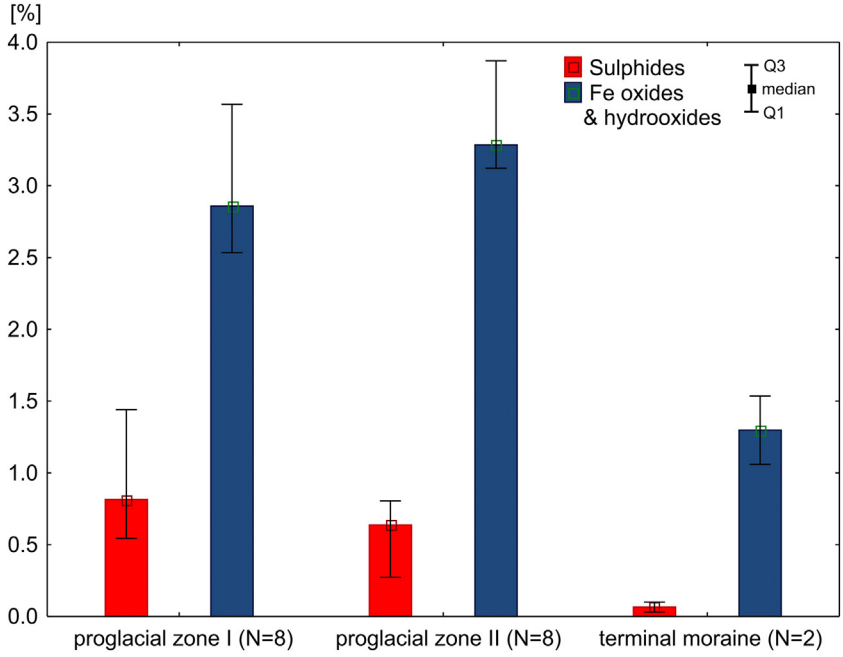

Fig. 7. Content of sulphides and iron oxides and hydrooxides in chronosequence of Werenskioldbreen proglacial zone based on QEMSCAN®.

Table 3
Geochemical indices of meltwater at the hydrometric stations at Werenskioldbreen (HSW).

Index	Werenskioldbreen		
	HSW early	HSW peak	HSW late
Sulphate mass fraction (**mean**, min-max)	**0.36**	**0.23**	**0.37**
	0.27–0.45	0.14–0.35	0.3–0.44
$*Na^+ + *K^+ / *Ca^{2+} + *Mg^{2+}$	**0.01**	**0.01**	**0.02**
(**mean**, min-max)	0.001–0.014	0.001–0.02	0.011–0.045

to the subglacial outflows (r = ~0.5–0.6, rho = ~0.5–0.7) (Fig. 8C, Table A.3).

The annual specific runoff from Werenskioldbreen in 2011 was 1.8 m, whereas the total solute mass flux corrected for atmospheric input was 121.9 t km^{-2} $year^{-1}$ (Stachnik et al., 2016) (Fig. A.10). The discharge characteristics at the hydrometric station showed clear seasonal changes from snowmelt at the beginning of season through peak flow in mid-summer and elevated discharge during summer/autumn transition (Fig. A.10).

5. Discussion

Our study provides insights into environmental conditions affecting the biogeochemical processes associated with sediment and proglacial water interactions as a consequence of glacier recession. We collected a wide range of SEM-EDS and XRD data supplemented with water chemistry in the proglacial area of Werenskioldbreen, an intensively glacierised basin in the High Arctic of Svalbard. Catchment lithology with easily weatherable minerals (e.g., carbonates, sulphides), very sparse vegetation cover and harsh climatic conditions make the Werenskioldbreen basin an endmember representative of the early stage of glacier retreat. Future climatic changes occurring on Svalbard, as well as in the Arctic, will likely result in more precipitation and higher air temperature (Førland et al., 2011; Hanssen-Bauer et al., 2019; Isaksen et al., 2016; Nordli et al., 2014; Przybylak and Wyszyński, 2019; Wawrzyniak and Osuch, 2019) and will further enhance biogeochemical cycles in glacierised basins.

5.1. Chemical weathering from proglacial sediments to meltwater

Physical weathering at sub-microscopic scale, which is an important process enhancing mineral dissolution and further subaerial solute transfer to proglacial streams, is clearly visible in the proglacial sediments of Werenskioldbreen. Our SEM-EDS analysis provides evidence of abrasion and fracturing that affected not only minerals vulnerable to weathering such as biotite and calcite, but also more resistant minerals such as albite and quartz (Figs. 3E-H). These processes likely caused fragmentation of the material into micron-sized particles (Hart, 2017) and alterations related to frost shattering (Figs. 3D-H). This latter is seen as intense weathering of porous, cracked rocks with foliation, layered shale/schist, or mineral veins (Lubera and Krzaklewski, 2020; Price and Velbel, 2014; Ruedrich et al., 2011). The varied thermal expansion of the minerals comprising the rock mass and their hardness, elasticity, and cleavage (e.g., micas) could also be important controls on weathering intensity. Production of fresh mineral surfaces and the larger specific surface area of minerals result from the physical weathering.

Table 4
Slopes and Pearson's correlation coefficients of ion associations (see Fig. 3A,B) in glacial meltwater at the hydrometric stations at Werenskioldbreen (HSW). Analyses of pre-assumption of linear regression models are shown in Table A.3. Italic depicts regression model with residuals violating an assumption of the model (lack of serial autocorrelation).

Ion association	HSW early (N = 57)	HSW peak (N = 100)	HSW late (N = 26)
$*Na^+ + *K^+$ vs. HCO_3^-	y = −2.9 + 0 .024*x;	$y = 8.848 * 10^{0.000597*x}$	y = -22.6 + 0.103*x
	(r = 0.32, $p < 0.05$)	($r = 0.22$, $p < 0.05$)	(r = 0.77, $p < 0.001$)
$*Na^+ + *K^+$ vs. $*SO_4^{2-}$	y = 4.3 + 0 .025*x	$y = 15.1 + 0.048*x$	y = 3.1 + 0.113*x;
	(r = 0.41, $p < 0.005$)	($r = 0.24$, $p < 0.05$)	(r = 0.75, $p < 0.001$)

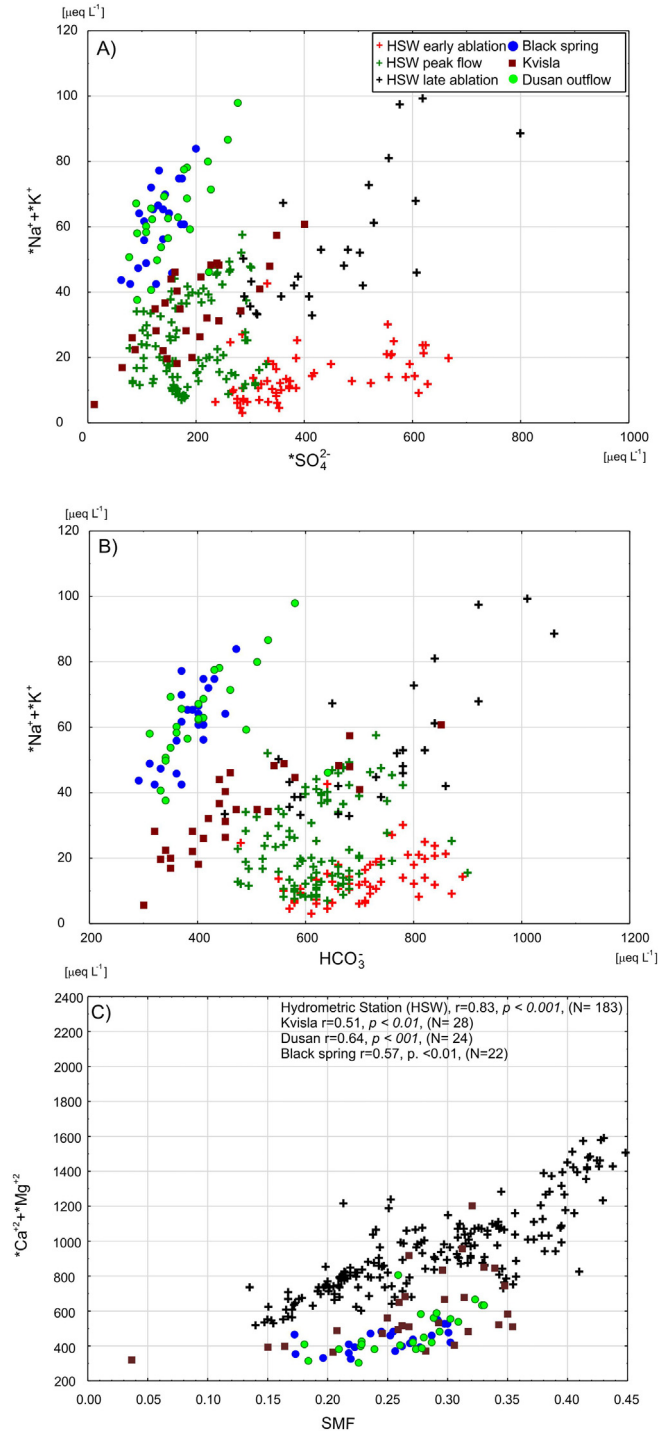

Fig. 8. Relationships between major ions and hydrochemical indices for the study area in Werenskioldbreen: (A) $*Na^+ + *K^+$ vs. $*SO_4^{2-}$, (B) $*Na^+ + *K^+$ vs. HCO_3^- (C) sulphate mass fraction (SMF) vs. $*Ca^{2+} + *Mg^2$. HSW denotes the hydrometric stations at Werenskioldbreen. Analyses of linear regression models and correlation coefficients are shown in Table A.3.

Physical weathering and water saturation enhance sulphide oxidation and carbonate dissolution. Sulphide minerals in the terminal moraine with an advanced degree of oxidation represent the long-term chemical alterations (Figs. 4I-J, 5E-F, A.8). This is consistent with previous observations of slow rates of chemical weathering due to a low level of physical weathering in diamictons (Brown et al., 1996). In contrast, chemical weathering in the proglacial area leads to intensive leaching of peripheral sulphur from sulphide minerals, which causes partial (e.g., Figs. 4E-F, 4H, 5C-D; Fig. A.4) and complete transformation of sulphides leading to the formation of Fe oxides (Figs. A.5, A.6, A.8). Our results show that weathering rims around weathered Fe sulphide grains are depleted in sulphur (Figs. 4, 5 and 6; Table 2). This indicates that sulphur is released as a sulphate to sediment pore waters and then to proglacial meltwater (Fig. 8C) (Szynkiewicz et al., 2013). Microfractures and microcracks forming as result of physical weathering in the subglacial environment and in the proglacial area favour leaching of sulphur and advancing sulphide oxidation (Fig. 4D, H). Despite the shorter exposure age, sulphide oxidation and carbonate dissolution are more advanced in the proglacial zones I and II as compared to the terminal moraine (Figs. 3C-D, A.1). This is likely related with a smaller grain fraction in the sediments (higher specific surface area), physical weathering, and relatively higher water saturation of sediments in glacier foreland. In addition, carbonate dissolution results in lowering the abundance of these minerals along the chronosequence (i.e., younger deposits in the proglacial zone and older deposits at the terminal moraine). The XRD analyses showed that carbonates are less abundant in samples from the terminal moraine than in samples from the proglacial zone (Fig. 2 and Table A.1.). This indicates that the advancement of weathering processes leads to the dissolution of carbonates facilitated by sulphuric acid originating from sulphide oxidation.

Sulphide oxidation enhances dissolution of carbonates in freshly exposed glaciofluvial sediments in the proglacial areas of receding glaciers. The SEM-EDS images of sediments collected in front of Werenskioldbreen show clear signs of sulphide oxidation at young sites situated in the vicinity of the glacier margin and large pyrite grains (Figs. 4A-B) to partially or totally dissolved pyrite in older profiles located farther away from the glacier margin (Figs. 4J-K, 5C-D, A.2, A.8). Sulphur is readily leached via sulphide oxidation, while Fe oxides form weathering rims around former sulphide grains (Auqué et al., 2019; Kwaśniak-Kominek et al., 2016; Rzepa et al., 2019; Uzarowicz, 2013) and the mobilised Fe recrystallises around other mineral grains. Furthermore, meltwater chemistry mimics sediment alteration because of a stronger coupling between carbonate derived ions ($*Ca^{2+} + *Mg^{2+}$) and SMF at the hydrometric station (Fig. 8C), and enrichment in bicarbonate and sulphate ions in the proglacial zone (Stachnik et al., 2016). The final step of sulphide dissolution is the formation of Fe oxide pseudomorphs characterised by total depletion of sulphur (Fig. A.5), which is in line with water saturation with respect to Fe hydroxide (Stachnik et al., 2019). Moreover, evident Fe oxide rims develop around Fe sulphide framboids as weathering proceeds in the terminal moraine (Fig. 6E-F). When compared to the proglacial area, the terminal moraine environment is more stable with less physical (e.g., glacier abrasion) and chemical (e.g., lower content of water) weathering (Fig. 4I-K).

Water chemistry links well with the chemical weathering of proglacial sediments at the early stage of glacier recession. The significant positive correlation between $*Ca^{2+} + *Mg^{2+}$ and SMF (Fig. 8C) shows that carbonate minerals are actively dissolved via sulphuric acid from sulphide oxidation (Figs. 4, 7, A.3, A.4), and leaching of carbonate minerals (Fig. A.7) was widely observed in the proglacial area of Werenskioldbreen. This is also in accordance to the slope of relationship between $*Ca^{2+} + *Mg^{2+}$ and SO_4^{2-} in meltwater from Werenskioldbreen (Stachnik et al., 2016) and other studies in alpine regions (Tranter et al., 2002; Wadham et al., 2010a; Yu et al., 2021). Carbonate dissolution and some dissolution of Mg–Ca-sulphate salts formed by freeze concentration and evaporative concentration are additionally responsible for a seasonal evolution of the chemical composition in pore water in the proglacial area (Cooper et al., 2011; Deuerling et al., 2018; Harmon et al., 2021; Szynkiewicz et al., 2013). Rising groundwater table in the proglacial area intensifies sulphide and carbonate dissolution, thereby causing elevated Ca^{2+}, Mg^{2+}, and SO_4^{2-} in meltwater (Stachnik et al., 2016). Weathering of Fe sulphide grains in the proglacial area is associated with a decrease in sulphide content in proglacial sediments (Fig. 7) and observations of a higher proportion of SO_4^{2-} ions in glacial meltwater (Fig. 8A). This observation is consistent with reports from previous proglacial geochemistry studies confirming that time of aerial exposure (age) is positively correlated with rates of mineral dissolution (Anderson et al., 2000; Scribner et al., 2015). Silicate

weathering is coupled with sulphide oxidation (Fig. 8A, Table 4) but this process is less pronounced compared to carbonate dissolution. SEM analyses show that Fe sulphide oxidation producing sulphuric acid occurs near aluminosilicates grains (Figs. 4E-H) (Wadham et al., 2010b). However, there is a lack of dissolution of aluminosilicate observed by the SEM-EDS and the ratio of silicate to carbonate-derived ions ($*Na^+ + *K^+$):($*Ca^{2+} + *Mg^{2+}$) in meltwater is an order of magnitude lower than other glacierised basins underlain by metasedimentary rocks (Stachnik et al., 2014; Wadham et al., 2010b). This suggests that although silicate weathering occurs, carbonate weathering appears to be more significant. To sum up, the observations from the hydrochemistry are in line with our SEM-EDS results of sediments from the proglacial zone, where oxidation of sulphides, although these minerals are minor mineral constituent of the sediments in the study area, supplies water with sulphuric acid that is mainly used as a proton donor for carbonate dissolution.

5.2. Biogeochemistry in the early stages of glacier recession

Our study shows that meltwater chemistry exhibits a clear signal of sulphide oxidation in proglacial sediments during the early stages of land-based glacier recession. This is consistent with previous studies from the Alps and the Himalayas, which showed geochemical alteration of sediments such as carbonate and sulphide weathering and the formation of clay minerals during the early stages of deglaciation (Deuerling et al., 2019; Mavris et al., 2010; Mavris et al., 2012; Vilmundardóttir et al., 2014; Zhou et al., 2016), although a link to meltwater chemistry has rarely been addressed (Anderson et al., 2000). At Werenskioldbreen, we found that dissolution of carbonates and sulphide oxidation in the proglacial area have a significant impact on enrichment of solute derived from both processes, although carbonates and sulphides are not abundant constituents of deposits in the study area. Studies focussing on glacier meltwater hydrochemistry have demonstrated the importance of sulphide oxidation from basins with diverse bedrock geology in the Himalayas (Li et al., 2019; Shukla et al., 2018; Yu et al., 2021), whereas chemical weathering under subglacial conditions beneath the Greenland Ice Sheet showed a strong impact of silicate weathering in spite of presence of low quantities of carbonates and sulphides (Graly et al., 2014; Moore et al., 2013). Iron sulphide oxidation, which is often microbially mediated (Borin et al., 2010; Skidmore et al., 2000), likely enhances formation of Fe oxide rims on mineral grains (Figs. A.3–4, A.8). As time progresses, Fe sulphide oxidation may be followed by grain entrainment or precipitation of Fe oxyhydroxides on suspended sediments (Stachnik et al., 2019) and further glaciofluvial erosion leading to export of reactive bio-available Fe species to downstream ecosystems.

Our study finds that leaching of Fe-bearing minerals and formation of iron hydroxide is strongest at the early stages of glacier recession (up to ~100 years) suggesting enhanced release of iron species to meltwater. The content of Fe-bearing minerals, such as sulphides and iron oxides hydroxides, are highest in the part of the proglacial area exposed from ice less than ~60 years ago, and substantially decreased at the terminal moraine from LIA (Fig. 7). Also, the grain size of sulphides diminishes as oxidation progresses along micro-cracks in minerals (Fig. 6). This links well with the transfer of solutes from sulphide oxidation and carbonate dissolution to meltwater (Fig. 8). This shows that longer exposure and leaching diminish the Fe oxides and hydroxides (e.g., at the terminal moraine) and likely lead to decrease in Fe supply to downstream ecosystem (Fig. 8). The micronutrient (e.g., iron including high share of Fe^{2+} (Hawkings et al., 2018; van Genuchten et al., 2021)) release via glaciofluvial erosion (sediment-bound fraction) and, to lesser extent, leaching (dissolved fraction) to meltwater appear to be important during the early stages of glacier recession. Similarly to iron release, during the early stages of glacier recession high bioavailability of organic matter species have been suggested (Holt et al., 2021). This mass flux at the early stages of glacier recession intensifies atmospheric CO_2 consumption via the carbon pump related to enhanced primary production in downstream iron-deficient aquatic ecosystems. Dissolution of carbonates via sulphuric acid in the proglacial zone causes a direct release to the atmosphere (Koelling et al., 2019; Torres et al., 2014, 2017). Despite of a minor importance of this process in small glaciers, it should be taken into account when dealing with biogeochemical processes at the early stage of recession (Graly et al., 2017). In conclusion, intense chemical weathering of Fe-bearing mineral enhances leaching and entrainment of highly bioavailable Fe in solution and as sediment-bond species.

Our study emphasizes the usefulness of applying XRD and SEM-EDS analyses of mineral surfaces in combination with water chemistry to conduct biogeochemical studies in front of receding glaciers. While observations of chemical weathering of sediments support glacier meltwater chemistry composition in the proglacial area, this relationship may be more complex in other glacial environments such as at the terminal moraine. In future studies on biogeochemical cycles in glacial environments, proglacial sediment-water chemistry interactions should be considered in more detail by analysing processes controlling chemical weathering in nanoscale using, for example, geochemical modelling of pore water and electron microprobe analyses of thin sections from undisturbed sediment samples.

6. Conclusions

This study provides combined hydrochemical, mineralogical (XRD), and scanning electron microscopy (SEM-EDS) evidence for a strong biogeochemical coupling between proglacial sediments and meltwater chemistry during the early stages of glacier recession (<100 years).

During the early stages of glacier recession biogeochemical processes are intensified in the proglacial area as sulphide oxidation and carbonate dissolution of proglacial sediments have a strong impact on meltwater chemistry in glacial streams. Water saturation and intense physical weathering enhance oxidation and further weathering of Fe sulphide grains resulting in the formation of secondary Fe oxide. The results infer that physical processes (e.g., cracking, fracturing, and frost shattering) associated with chemical weathering of mineral grains increase the dissolution rate. The weathering is particularly intense immediately after deglaciation because of intensive mineral and chemical transformations related with the adjustment of the sediment mineral assemblages to the environmental conditions. The leached solutes are transferred to glacial meltwater and affecting the biogeochemical composition via delivery of chemically reactive Fe species to aquatic ecosystems. The early stages of glacial recession play an important role in biogeochemical cycles of bioavailable elements enhanced by the coupling between proglacial sediment weathering and solute transport in meltwater.

Supplementary data to this article can be found online at https://doi.org/10.1016/j.scitotenv.2022.155383.

Funding

This work was supported by the National Science Centre in Poland [grant number no N306 792040]; The Research Council of Norway Arctic Field Grant 2012 [grant number 1885]; and statutory funds of the Institute of Geography and Spatial Management at the Jagiellonian University, Poland, Centre for Polar Studies KNOW (Leading National Research Centre) of the University of Silesia (Poland), and the Łukasiewicz Research Network, PORT Polish Centre for Technology Development, Poland.

CRediT authorship contribution statement

Łukasz Stachnik: Conceptualization, Writing – original draft, Investigation, Formal analysis. **Jacob C. Yde:** Writing – review & editing, Conceptualization. **Kazimierz Krzemień:** Conceptualization, Resources. **Łukasz Uzarowicz:** Visualization, Resources, Writing – original draft. **Sławomir Sitek:** Visualization, Project administration. **Piotr Kenis:** Methodology, Investigation.

Declaration of competing interest

The authors declare that they have no known competing financial interests or personal relationships that could have appeared to influence the work reported in this paper.

Acknowledgement

We thank our colleagues from the research projects for their help during the fieldwork in the Svalbard. We also thank Michał Łopuch for preparing the satellite images of the study area and Emilia Lepianka for the graphical visualisations. We would like to thank two anonymous reviewers for the thorough review.

References

Anderson, J.N., Saros, J.E., Bullard, J.E., Cahoon, S.M.P., Mcgowan, S., Bagshaw, E.A., Barry, C.D., Bindler, R., Burpee, B.T., Carrivick, J.L., Fowler, R.A., Fox, A.D., Fritz, S.C., Giles, M.E., Hamerlik, L., Ingeman-Nielsen, T., Law, A.C., Mernild, S.H., Northington, R.M., Osburn, C.L., Pla-Rabès, S., Post, E., Telling, J., Stroud, D.A., Whiteford, E.J., Yallop, M.L., Yde, J.C., 2017. The Arctic in the twenty-first century: changing biogeochemical linkages across a paraglacial landscape of Greenland. BioScience 67, 118–133. https://doi.org/10.1093/biosci/biw158.

Anderson, S.P., Drever, J.I., Frost, C.D., Holden, P., 2000. Chemical weathering in the foreland of a retreating glacier. Geochim. Cosmochim. Acta 64, 1173–1189. https://doi.org/10.1016/s0016-7037(99)00358-0.

Andrews, M.G., Jacobson, A.D., 2018. Controls on the solute geochemistry of subglacial discharge from the Russell Glacier, Greenland Ice Sheet determined by radiogenic and stable Sr isotope ratios. Geochim. Cosmochim. Acta 239, 312–329. https://doi.org/10.1016/j.gca.2018.08.004.

Arrigo, K.R., van Dijken, G.L., Castelao, R.M., Luo, H., Rennermalm, Å.K., Tedesco, M., Mote, T.L., Oliver, H., Yager, P.L., 2017. Melting glaciers stimulate large summer phytoplankton blooms in southwest Greenland waters. Geophys. Res. Lett. 44, 6278–6285. https://doi.org/10.1002/2017gl073583.

Auqué, L.F., Puigdomenech, I., Tullborg, E.L., Gimeno, M.J., Grodzinsky, K., Hogmalm, K.J., 2019. Chemical weathering in a moraine at the ice sheet margin at Kangerlussuaq, western Greenland. Arct. Antarct. Alp. Res. 51, 440–459. https://doi.org/10.1080/15230430.2019.1660125.

Bernasconi, S.M., Bauder, A., Bourdon, B., Brunner, I., Bünemann, E., Christl, I., Derungs, N., Edwards, P., Farinotti, D., Frey, B., Frossard, E., Furrer, G., Gierga, M., Göransson, H., Gülland, K., Hagedorn, F., Hajdas, I., Hindshaw, R., Ivy-Ochs, S., Jansa, J., Jonas, T., Kiczka, M., Kretzschmar, R., Lemarchand, E., Luster, J., Magnusson, J., Mitchell, E.A.D., Venterink, H.O., Plötze, M., Reynolds, B., Smittenberg, R.H., Stähli, M., Tamburini, F., Tipper, E.T., Wacker, L., Welc, M., Wiederhold, J.G., Zeyer, J., Zimmermann, S., Zumsteg, A., 2011. Chemical and biological gradients along the Damma glacier soil chronosequence, Switzerland. Vadose Zone J. 10, 867–883. https://doi.org/10.2136/vzj2010.0129.

Bhatia, M.P., Kujawinski, E.B., Das, S.B., Breier, C.F., Henderson, P.B., Charette, M.A., 2013. Greenland meltwater as a significant and potentially bioavailable source of iron to the ocean. Nat. Geosci. 6, 274–278. https://doi.org/10.1038/ngeo1746.

Borin, S., Ventura, S., Tambone, F., Mapelli, F., Schubotz, F., Brusetti, L., Scaglia, B., D'Acqui, L., Solheim, B., Turicchia, S., Marasco, R., Hinrichs, K., Baldi, F., Adani, F., Daffonchio, D., 2010. Rock weathering creates oases of life in a high Arctic desert. Environ. Microbiol. 12 (2), 293–303. https://doi.org/10.1111/j.1462-2920.2009.02059.x.

Brown, G.H., Tranter, M., Sharp, M.J., 1996. Experimental investigations of the weathering of suspended sediment by alpine glacial meltwater. Hydrol. Process. 10, 579–597. https://doi.org/10.1002/(SICI)1099-1085(199604)10:4<579::AID-HYP393>3.0.CO;2-D.

Christiansen, J.R., Röckmann, T., Popa, M.E., Sapart, C.J., Jørgensen, C.J., 2021. Carbon Emissions From the Edge of the Greenland Ice Sheet Reveal Subglacial Processes of Methane and Carbon Dioxide Turnover. J. Geophys. Res-Biogeo. 126. https://doi.org/10.1029/2021JG006308 e2021JG006308.

Ciężkowski, W., Głowacki, T., Grudzińska, K., Kasza, D., Zagożdżon, P., 2018. Front of the Werenskiold Glacier (Svalbard) – Changes in Years 1957–2013. EPJ Web of Conferences, 29. Web of Conferences, 00030.

Cooper, R., Hodgkins, R., Wadham, J., Tranter, M., 2011. The hydrology of the proglacial zone of a high-Arctic glacier (Finsterwalderbreen, Svalbard): sub-surface water fluxes and complete water budget. J. Hydrol. 406, 88–96. https://doi.org/10.1016/j.jhydrol.2011.06.008.

Cooper, R.J., Wadham, J.L., Tranter, M., Hodgkins, R., Peters, N.E., 2002. Groundwater hydrochemistry in the active layer of the proglacial zone, Finsterwalderbreen, Svalbard. J. Hydrol. 269, 208–223. https://doi.org/10.1016/s0022-1694(02)00279-2.

Czerny, J., Lipień, G., Manecki, A., Piestrzyński, A., 1992. Geology and ore-mineralization of the Hecla Hoek Succession (Precambrian) in front of Werenskioldbreen, south Spitsbergen. Stud. Geol. Pol. 98, 67–113.

Czerny, J., Kieres, A., Manecki, M., Rajchel, J., 1993. Geological Map of the SW Part of Wedel-Jarlsberg Land, Spitsbergen. In: Manecki, A. (Ed.), Institute of Geology and Mineral Deposits, University of Mining and Metallurgy, Kraków, Poland.

Deuerling, K.M., Martin, J.B., Martin, E.E., Scribner, C.A., 2018. Hydrologic exchange and chemical weathering in a proglacial watershed near Kangerlussuaq, west Greenland. J. Hydrol. 556, 220–232. https://doi.org/10.1016/j.jhydrol.2017.11.002.

Deuerling, K.M., Martin, J.B., Martin, E.E., Abermann, J., Myreng, S.M., Petersen, D., Rennermalm, Å.K., 2019. Chemical weathering across the western foreland of the Greenland Ice Sheet. Geochim. Cosmochim. Acta 245, 426–440. https://doi.org/10.1016/j.gca.2018.11.025.

Eiriksdottir, E.S., Gislason, S.R., Oelkers, E.H., 2015. Direct evidence of the feedback between climate and nutrient, major, and trace element transport to the oceans. Geochim. Cosmochim. Acta 166, 249–266. https://doi.org/10.1016/j.gca.2015.06.005.

Førland, E.J., Benestad, R., Hanssen-Bauer, I., Haugen, J.E., Skaugen, T.E., 2011. Temperature and precipitation development at Svalbard 1900–2100. Adv. Meteor. 893790. https://doi.org/10.1155/2011/893790.

van Genuchten, C.M., Rosing, M.T., Hopwood, M.J., Liu, T., Krause, J., Meire, L., 2021. Decoupling of particles and dissolved iron downstream of Greenlandic glacier outflows. Earth Planet. Sc. Lett. 576, 117234. https://doi.org/10.1016/j.epsl.2021.117234.

Gerringa, L.J.A., Alderkamp, A.C., Laan, P., Thuróczy, C.E., De Baar, H.J.W., Mills, M.M., van Dijken, G.L., Haren, H.V., Arrigo, K.R., 2012. Iron from melting glaciers fuels the phytoplankton blooms in Amundsen Sea (Southern Ocean): iron biogeochemistry. Deep-Sea Res. Pt. II 71-76, 16–31. https://doi.org/10.1016/j.dsr2.2012.03.007.

Gíslason, S.R., Oelkers, E.H., Snorrason, Á., 2006. Role of river-suspended material in the global carbon cycle. Geology 34, 49–52. https://doi.org/10.1130/G22045.1.

Grabiec, M., Budzik, T., Głowacki, P., 2012. Modeling and hindcasting of the mass balance of werenskioldbreen (Southern Svalbard). Arct. Anatarct. Alp. Res. 44, 164–179. https://doi.org/10.1657/1938-4246-44.2.164.

Graly, J.A., Humphrey, N.F., Landowski, C.M., Harper, J.T., 2014. Chemical weathering under the Greenland ice sheet. Geology 42, 551–554. https://doi.org/10.1130/g35370.1.

Graly, J.A., Drever, J.I., Humphrey, N.F., 2017. Calculating the balance between atmospheric CO2 drawdown and organic carbon oxidation in subglacial hydrochemical systems. Glob. Biogeochem. Cycles 31, 709–727. https://doi.org/10.1002/2016GB005425.

Hagen, J.O., Liestøl, O., Roland, E., Jørgensen, T., 1993. Glacier atlas of Svalbard and Jan Mayen. Meddelelser 129. Norsk Polarinstitutt, Oslo.

Hanssen-Bauer, I., Førland, E., Hisdal, H., Mayer, S., Sandø, A., Sorteberg, A., Adakudlu, M., Andresen, J., Bakke, J., Beldring, S., Benestad, R., van der Bilt, W., Bogen, J., Borstad, C., Breili, K., Breivik, O., Børsheim, K., Christiansen, H., Dobler, A., Wong, W., 2019. Climate in Svalbard 2100 Editors -A Knowledge Base for Climate Adaptation. Norwegian Centre for Climate Services.

Harmon, R., Leslie, D., Lyons, W., Welch, K., McKnight, D., 2021. Geochemistry of contrasting stream types, Taylor Valley, Antarctica. Geol. Soc. Am. Bull. 133 (1–2), 425–448. https://doi.org/10.1130/b35479.1.

Hart, J.K., 2017. Subglacial till formation: microscale processes within the subglacial shear zone. Quat. Sci. Rev. 170, 26–44. https://doi.org/10.1016/j.quascirev.2017.06.021.

Hasholt, B., Van As, D., Mikkelsen, A.B., Mernild, S., Yde, J.C., 2018. Observed sediment and solute transport from the Kangerlussuaq sector of the Greenland ice sheet (2006-2016). Arc. Antarct. Alp. Res. 50, S100009. https://doi.org/10.1080/15230430.2018.1433789.

Hawkings, J., Benning, L., Raiswell, R., Kaulich, B., Araki, T., Abyaneh, M., Stockdale, A., Koch-Müller, M., L Wadham, J., Tranter, M., 2018. Biolabile ferrous iron bearing nanoparticles in glacial sediments. Earth Planet. Sci. Lett. 493, 92–101. https://doi.org/10.1016/j.epsl.2018.04.022.

Hawkings, J.R., Wadham, J.L., Tranter, M., Raiswell, R., Benning, L.G., Statham, P.J., Tedstone, A., Nienow, P., Lee, K., Telling, J., 2014. Ice sheets as a significant source of highly reactive nanoparticulate iron to the oceans. Nat. Commun. 5, 1–8. https://doi.org/10.1038/ncomms4929.

Hawkings, J.R., Wadham, J.L., Benning, L.G., Hendry, K.R., Tranter, M., Tedstone, A., Nienow, P., Raiswell, R., 2017. Ice sheets as a missing source of silica to the polar oceans. Nat. Commun. 8, 14198. https://doi.org/10.1038/ncomms14198.

Hodson, A., Tranter, M., Vatne, G., 2000. Contemporary rates of chemical denudation and atmospheric CO_2 sequestration in glacier basins: an Arctic perspective. Earth Surf. Process. Landf. 25, 1447–1471. https://doi.org/10.1002/1096-9837(200012)25:13<1447::aid-esp156>3.0.co;2-9.

Hodson, A.J., Yde, J.C., 2022. The geochemistry of glacial meltwaters. In: Shroder, J.J.F. (Ed.), Treatise on Geomorphology. 4. Elsevier, Academic Press, pp. 290–304.

Hodson, A.J., Nowak, A., Sabacka, M., Jungblut, A., Navarro, F., Pearce, D., Avila-Jimenez, M.L., Convey, P., Vieira, G., 2017. Climatically sensitive transfer of iron to maritime Antarctic ecosystem by surface runoff. Nat. Commun. 8, 14499. https://doi.org/10.1038/ncomms14499.

Holland, H.D., 1978. The Chemistry of the Atmosphere and Oceans. Wiley Intersciece, New York.

Holt, A., Fellman, J., Hood, E., Kellerman, A., Raymond, P., Stubbins, A., Dittmar, T., Spencer, R., 2021. The evolution of stream dissolved organic matter composition following glacier retreat in coastal watersheds of southeast Alaska. Biogeochemistry https://doi.org/10.1007/s10533-021-00815-6.

Hopwood, M.J., Carroll, D., Dunse, T., Hodson, A., Holding, J.M., Iriarte, J.L., Ribeiro, S., Achterberg, E.P., Cantoni, C., Carlson, D.F., Chierici, M., Clarke, J.S., Cozzi, S., Fransson, A., Juul-Pedersen, T., Winding, M.H.S., Meire, L., 2020. Review article: how does glacier discharge affect marine biogeochemistry and primary production in the Arctic? Cryosphere 14, 1347–1383. https://doi.org/10.5194/tc-14-1347-2020.

Isaksen, K., Nordli, Ø., Førland, E.J., Łupikasza, E., Eastwood, S., Niedźwiedź, T., 2016. Recent warming on Spitsbergen—influence of atmospheric circulation and sea ice cover. J. Geophys. Res.-Atmos. 121, 11,913–11,931. https://doi.org/10.1002/2016jd025606.

Kabala, C., Zapart, J., 2012. Initial soil development and carbon accumulation on moraines of the rapidly retreating Werenskiold Glacier, SW Spitsbergen, Svalbard archipelago. Geoderma 175-176, 9–20. https://doi.org/10.1016/j.geoderma.2012.01.025.

Kenis, P., Skurzyński, J., Jary, Z., Kubik, R., 2020. A new methodological approach (QEMSCAN®) in the mineralogical study of Polish loess: guidelines for further research. Open Geosci. 12, 342–353. https://doi.org/10.1515/geo-2020-0138.

Koelling, M., Bouimetarhan, I., Bowles, M., Felis, T., Goldhammer, T., Hinrichs, K.-U., Schulz, M., Zabel, M., 2019. Consistent CO_2 release by pyrite oxidation on continental shelves

prior to glacial terminations. Nat. Geosci. 12, 929–934. https://doi.org/10.1038/s41561-019-0465-9.
Kwaśniak-Kominek, M., Manecki, M., Rzepa, G., Płonka, A.M., Górniak, D., 2016. Weathering in a regolith on the Werenskioldbreen forefield (SW spitsbergen): modelling of pore water chemistry. Ann. Soc. Geol. Pol. 86, 249–264. https://doi.org/10.14241/asgp.2016.014.
Li, X., Ding, Y., Liu, Q., Zhang, Y., Han, T., Jing, Z., Yu, Z., Li, Q., Liu, S., 2019. Intense chemical weathering at glacial meltwater-dominated Hailuogou basin in the southeastern Tibetan Plateau. Water-Sui. 11 (6), 1209. https://doi.org/10.3390/w11061209.
Lubera, E., Krzaklewski, P., 2020. Wietrzenie mrozowe wybranych skał tatrzańskich w świetle badań laboratoryjnych. Przegl. Geogr. 92, 19–39. https://doi.org/10.7163/PrzG.2020.1.2.
Majchrowska, E., Ignatiuk, D., Jania, J., Marszałek, H., Wąsik, M., 2015. Seasonal and interannual variability in runoff from the Werenskioldbreen catchment, Spitsbergen. Pol. Polar Res. 36, 197–224. https://doi.org/10.1515/popore-2015-0014.
Marsz, A.A., Styszyńska, A., 2013. Climate and Climate Change at Hornsund, Svalbard. Gdynia Maritime University, Gdynia (Poland).
Mavris, C., Egli, M., Plötze, M., Blum, J.D., Mirabella, A., Giaccai, D., Haeberli, W., 2010. Initial stages of weathering and soil formation in the Morteratsch proglacial area (Upper Engadine, Switzerland). Geoderma 155, 359–371. https://doi.org/10.1016/j.geoderma.2009.12.019.
Mavris, C., Götze, J., Plötze, M., Egli, M., 2012. Weathering and mineralogical evolution in a high Alpine soil chronosequence: a combined approach using SEM-EDX, cathodoluminescence and Nomarski DIC microscopy. Sediment. Geol. 280, 108–118. https://doi.org/10.1016/j.sedgeo.2012.04.008.
Meire, L., Mortensen, J., Rysgaard, S., Bendtsen, J., Boone, W., Meire, P., Meysman, F.J.R., 2016. Spring bloom dynamics in a subarctic fjord influenced by tidewater outlet glaciers (Godthåbsfjord, SW Greenland). J. Geophys. Res. Biogeosci. 121, 1581–1592. https://doi.org/10.1002/2015JG003240.
Moore, J., Jacobson, A.D., Holmden, C., Craw, D., 2013. Tracking the relationship between mountain uplift, silicate weathering, and long-term CO_2 consumption with Ca isotopes: Southern Alps, New Zealand. Chem. Geol. 341, 110–127. https://doi.org/10.1016/j.chemgeo.2013.01.005.
Nordli, Ø., Przybylak, R., Ogilvie, A.E.J., Isaksen, K., 2014. Long-term temperature trends and variability on Spitsbergen: the extended Svalbard Airport temperature series, 1898–2012. Polar Res. 33, 21349. https://doi.org/10.3402/polar.v33.21349.
Pereyma, J., Migała, K., Sikora, S., 2013. Geographical environment in the vicinity of the Stanisław Baranowski Polar Station - Werenskioldbreen: Climate. In: Zwoliński, Z., Kostrzewski, A., Pulina, M. (Eds.), Ancient and Modern Geoecosystems of Spitsbergen. Association of Polish Geomorphologists, Poznań, Poland, pp. 118–121.
Price, J.R., Velbel, M.A., 2014. Rates of biotite weathering, and clay mineral transformation and neoformation, determined from watershed geochemical mass-balance methods for the Coweeta Hydrologic Laboratory, Southern Blue Ridge Mountains, North Carolina, USA. Aquat. Geochem. 20, 203–224. https://doi.org/10.1007/s10498-013-9190-y.
Przybylak, R., Wyszyński, P., 2019. Air temperature changes in the Arctic in the period 1951–2015 in the light of observational and reanalysis data. Theor. Appl. Climatol. 139, 75–94. https://doi.org/10.1007/s00704-019-02952-3.
Ruedrich, J., Kirchner, D., Siegesmund, S., 2011. Physical weathering of building stones induced by freeze–thaw action: a laboratory long-term study. Environ. Earth Sci. 63, 1573–1586. https://doi.org/10.1007/s12665-010-0826-6.
Rzepa, G., Manecki, M., Jakubski, G., Kwaśniak-Kominek, M., Czerny, J., Górniak, D., 2019. Weathering in a regolith on the Werenskioldbreen Glacier forefield (SW Spitsbergen). 2. Speciation of Fe, Mn, Pb, Cu and Zn in the chronosequence. Ann. Soc. Geol. Pol. 89, 317–341. https://doi.org/10.14241/asgp.2019.06.
Saros, J.E., Anderson, N.J., Juggins, S., McGowan, S., Yde, J.C., Telling, J., Bullard, J.E., Yallop, M.L., Heathcote, A.J., Burpee, B.T., Fowler, R.A., Barry, C.D., Northington, R.M., Osburn, C.L., Pla-Rabes, S., Mernild, S.H., Whiteford, E.J., Andrews, M.G., Kerby, J.T., Post, E., 2019. Arctic climate shifts drive rapid ecosystem responses across the West Greenland landscape. Environ. Res. Lett. 14, 074027. https://doi.org/10.1088/1748-9326/ab2928.
Scribner, C.A., Martin, E.E., Martin, J.B., Deuerling, K.M., Collazo, D.F., Marshall, A.T., 2015. Exposure age and climate controls on weathering in deglaciated watersheds of western Greenland. Geochim. Cosmochim. Acta 170, 157–172. https://doi.org/10.1016/j.gca.2015.08.008.
Shukla, T., Sundriyal, S., Stachnik, L., Mehta, M., 2018. Carbonate and silicate weathering in glacial environments and its relation to atmospheric CO_2 cycling in the Himalaya. Ann. Glaciol. 59, 159–170. https://doi.org/10.1017/aog.2019.5.
Skidmore, M.L., Foght, J.M., Sharp, M.J., 2000. Microbial life beneath a high Arctic glacier. Appl. Environ. Microbiol. 66, 3214–3220. https://doi.org/10.1128/aem.66.8.3214-3220.2000.
Smetacek, V., Klaas, C., Strass, V.H., Assmy, P., Montresor, M., Cisewski, B., Savoye, N., Webb, A., d'Ovidio, F., Arrieta, J.M., Bathmann, U., Bellerby, R., Berg, G.M., Croot, P., Gonzalez, S., Henjes, J., Herndl, G.J., Hoffmann, L.J., Leach, H., Losch, M., Mills, M.M., Neill, C., Peeken, I., Röttgers, R., Sachs, O., Sauter, E., Schmidt, M.M., Schwarz, J., Terbrüggen, A., Wolf-Gladrow, D., 2012. Deep carbon export from a Southern Ocean iron-fertilized diatom bloom. Nature 487, 313–319. https://doi.org/10.1038/nature11229.
Stachnik, Ł., Wałach, P., Uzarowicz, Ł., Yde, J.C., Tosheva, Z., Wrońska-Wałach, D., 2014. Water chemistry and hydrometeorology in a glacierized catchment in the Polar Urals, Russia. J. Mt. Sci. 11, 1097–1111. https://doi.org/10.1007/s11629-014-3034-0.
Stachnik, Ł., Majchrowska, E., Yde, J.C., Nawrot, A., Cichała-Kamrowska, K., Ignatiuk, D., Piechota, A., 2016. Chemical denudation and the role of sulfide oxidation at Werenskioldbreen, Svalbard. J. Hydrol. 538, 177–193. https://doi.org/10.1016/j.jhydrol.2016.03.059.
Stachnik, Ł., Yde, J., Nawrot, A., Uzarowicz, Ł., Łepkowska, E., Kozak, K., 2019. Aluminium in glacial meltwater demonstrates an association with nutrient export (Werenskiöldbreen, Svalbard). Hydrol. Process. 33, 1638–1657. https://doi.org/10.1002/hyp.13426.
Szymański, W., 2017. Quantity and chemistry of water-extractable organic matter in surface horizons of Arctic soils under different types of tundra vegetation – A case study from the Fuglebergsletta coastal plain (SW Spitsbergen). Geoderma 305, 30–39. https://doi.org/10.1016/j.geoderma.2017.05.038.
Szymański, W., Maciejowski, W., Ostafin, K., Ziaja, W., Sobucki, M., 2019. Impact of parent material, vegetation cover, and site wetness on variability of soil properties in proglacial areas of small glaciers along the northeastern coast of Sørkappland (SE Spitsbergen). Catena 183, 104209. https://doi.org/10.1016/j.catena.2019.104209.
Szymański, W., Drewnik, M., Stolarczyk, M., Musielok, Ł., Gus-Stolarczyk, M., Skiba, M., 2022. Occurrence and stability of organic intercalation in clay minerals from permafrost-affected soils in the High Arctic – A case study from Spitsbergen (Svalbard). Geoderma 408, 115591. https://doi.org/10.1016/j.geoderma.2021.115591.
Szynkiewicz, A., Modelska, M., Buczyński, S., Borrok, D.M., Merrison, J.P., 2013. The polar sulfur cycle in the Werenskioldbreen, Spitsbergen: possible implications for understanding the deposition of sulfate minerals in the North Polar Region of Mars. Geochim. Cosmochim. Acta 106, 326–343. https://doi.org/10.1016/j.gca.2012.12.041.
Torres, M.A., West, A.J., Li, G., 2014. Sulphide oxidation and carbonate dissolution as a source of CO2 over geological timescales. timescales. Nature 507, 346–349. https://doi.org/10.1038/nature13030.
Torres, M.A., Moosdorf, N., Hartmann, J., Adkins, J.F., West, A.J., 2017. Glacial weathering, sulfide oxidation, and global carbon cycle feedbacks. Proc. Natl. Acad. Sci. USA 114, 8716–8721. https://doi.org/10.1073/pnas.1702953114.
Tranter, M., Sharp, M.J., Lamb, H.R., Brown, G.H., Hubbard, B.P., Willis, I.C., 2002. Geochemical weathering at the bed of Haut glacier d'Arolla, Switzerland - a new model. Hydrol. Process. 16, 959–993. https://doi.org/10.1002/hyp.309.
Uzarowicz, Ł., 2013. Microscopic and microchemical study of iron sulphide weathering in a chronosequence of technogenic and natural soils. Geoderma 197–198, 137–150. https://doi.org/10.1016/j.geoderma.2013.01.006.
Uzarowicz, L., Skiba, S., 2011. Technogenic soils developed on mine spoils containing iron sulphides: mineral transformations as an indicator of pedogenesis. Geoderma 163, 95–108. https://doi.org/10.1016/j.geoderma.2011.04.008.
Vilmundardóttir, O.K., Gísladóttir, G., Lal, R., 2014. Early stage development of selected soil properties along the proglacial moraines of Skaftafellsjökull glacier, SE-Iceland. Catena 121, 142–150. https://doi.org/10.1016/j.catena.2014.04.020.
Wadham, J.L., Tranter, M., Hodson, A.J., Hodgkins, R., Bottrell, S., Cooper, R., Raiswell, R., 2010. Hydro-biogeochemical coupling beneath a large polythermal Arctic glacier: implications for subice sheet biogeochemistry. J. Geophys. Res. 115, F04017. https://doi.org/10.1029/2009jf001602.
Wadham, J.L., Tranter, M., Skidmore, M., Hodson, A.J., Priscu, J., Lyons, W.B., Sharp, M., Wynn, P., Jackson, M., 2010. Biogeochemical weathering under ice: size matters. Glob. Biogeochem. Cycles 24, GB3025. https://doi.org/10.1029/2009gb003688.
Wawrzyniak, T., Osuch, M., 2019. 40 years High Arctic climatological dataset of the Polish Polar Station Hornsund (SW Spitsbergen, Svalbard). Earth Syst. Sci. Data 12, 805–815. https://doi.org/10.5194/essd-2019-222.
Weber, P., Stewart, W.A., Skinner, W.M., Weisener, C., Thomas, J., Smart, R.S.C., 2004. Geochemical effects of oxidation products and framboidal pyrite oxidation in acid mine drainage prediction techniques. Appl. Geochem. 19, 1953–1974. https://doi.org/10.1016/j.apgeochem.2004.05.002.
Wietrzyk-Pełka, P., Rola, K., Szymański, W., Węgrzyn, M.H., 2020. Organic carbon accumulation in the glacier forelands with regard to variability of environmental conditions in different ecogenesis stages of High Arctic ecosystems. Sci. Total. Environ. 717, 135151. https://doi.org/10.1016/j.scitotenv.2019.135151.
Yde, J.C., Knudsen, N.T., Hasholt, B., Mikkelsen, A.B., 2014. Meltwater chemistry and solute export from a Greenland Ice Sheet catchment, Watson River, West Greenland. J. Hydrol. 519, 2165–2179. https://doi.org/10.1016/j.jhydrol.2014.10.018.
Yu, Z., Wu, G., Li, F., Chen, M., Vi Tran, T., Liu, X., Gao, S., 2021. Glaciation enhanced chemical weathering in a cold glacial catchment, western Nyaingêntanglha Mountains, central Tibetan Plateau. J. Hydrol. 126197. https://doi.org/10.1016/j.jhydrol.2021.126197.
Zhou, J., Bing, H., Wu, Y., Yang, Z., Wang, J., Sun, H., Luo, J., Liang, J., 2016. Rapid weathering processes of a 120-year-old chronosequence in the Hailuogou Glacier foreland, Mt. Gongga, SW China. Geoderma 267, 78–91. https://doi.org/10.1016/j.geoderma.2015.12.024.
Zolkos, S., Tank, S.E., Kokelj, S.V., 2018. Mineral weathering and the permafrost carbon-climate feedback. Geophys. Res. Lett. 45, 9623–9632. https://doi.org/10.1029/2018gl078748.